THE LIFT DISTRIBUTION AND THE LIFT CURVE SLOPE FOR WING/BODY COMBINATIONS.

By: B. M. BLAIR.

SUMMARY.

An examination is made in this paper of a number of methods for calculating the spanwise load distribution on wing/body combinations. From the load distribution, values are then obtained for the lift curve slope. The most versatile method for solving this problem appears to be that proposed by Multhopp, and it is here described in detail, together with various extensions suggested by Weber, Kirby, and Kettle. This method is not very accurate for wings of aspect ratio of 2 or less, but it is very satisfactory for higher values of aspect ratio.

A DEUCE programme has been written to calculate the load distribution over the span using this method, and the calculation has been carried out for a large number of wings and wing/body combinations in which the aspect ratio, taper ratio, angle of sweep-back, and body size are the variables. From the load distributions so obtained, values of the lift curve slope were calculated and are shown in graphical form. To show the actual effect of the body, the ratio

$\left[\dfrac{\frac{dC_L}{d\alpha}(\text{combination})}{\frac{dC_L}{d\alpha}(\text{wing alone})}\right]$ was calculated for each case and these values are also shown in graphs. An attempt is then made to give some physical reasons for this body effect.

A short series of experimental tests was also carried out in a low speed wind tunnel on a number of rectangular wing/alone and wing/body models, and the lift curve slope was obtained for each case. These results, when given in the form $\left[\dfrac{\frac{dC_L}{d\alpha}(\text{combination})}{\frac{dC_L}{d\alpha}(\text{wing alone})}\right]$, are found to be in good agreement with the predicted values.

B.M.Blair.

THE LIFT DISTRIBUTION AND THE LIFT CURVE SLOPE FOR WING/BODY COMBINATIONS

by

B. M. BLAIR, B.Sc.

June, 1962.

SUMMARY.

An examination is made of a number of methods for calculating the spanwise load distribution on wing/body combinations. The method which appears to be most useful, that of Multhopp, is described in detail, together with various extensions suggested by Weber, Kirby, and Kettle. It is not very accurate for aspect ratios of 2 or less.

A DEUCE programme has been written to calculate the load distribution obtained by this method, and this calculation has been carried out for a large number of configurations with aspect ratio, sweep-back, taper ratio, and body size as the variables. From the load distribution so obtained, values were found for the lift curve slope, and these are given in a series of figures. By calculating the ratio $\left[\dfrac{\frac{dC_L}{d\alpha}\text{(combination)}}{\frac{dC_L}{d\alpha}\text{(wing alone)}}\right]$, which is plotted in another series of figures, some idea can be obtained of the effect which the body has on the wing, and an attempt is made to give some physical reasons for this effect.

A short series of experimental tests was also carried out in a low speed wind tunnel on a number of wing/alone and wing/body models, and the lift curve slope was obtained for each case. These results are found to be in good agreement with the predicted values.

LIST OF CONTENTS.

LIST OF SYMBOLS.

A	Aspect ratio $= \dfrac{(\text{span})^2}{(\text{gross wing area})}$.
a	Lift curve slope.
a_0	Two-dimensional lift curve slope.
b	Wing span.
c	Wing chord.
$\bar{c}$	Geometric mean wing chord.
$C_{L\alpha} = \dfrac{dC_L}{d\alpha}$	Lift curve slope.
D	Body diameter.
k	Wing thickness factor, equation (3.28).
k'	Taper ratio $= \dfrac{\text{tip chord}}{\text{centre chord}}$.
L	Total lift.
L'	Local spanwise lift.
R	Body radius.
$R\left(\dfrac{d\bar{u}}{du}\right)$	Real part of the differential quotient $\dfrac{d\bar{u}}{du}$.
t	Wing thickness.
V_0	Velocity of the free stream.
v_z	Total velocity component in the direction of the z-axis.
v_{z_B}	Additional downwash due to the effect of the body.
v_{z_i}	Induced downwash due to trailing vortices.
$v_{z_{iT}}$	Induced downwash in the Trefftz-plane.
x, y, z	Cartesian co-ordinates.

α_W	Angle of incidence of the wing to the free stream.
α_B	Angle of incidence of the body to the free stream.
α_{eff}	Effective angle of incidence.
α_i	Induced angle of incidence.
Γ	Circulation around the wing.
Γ_m	Circulation in the wing/body junction.
γ	Non-dimensional circulation = $\frac{\Gamma}{bV_0}$.
η	Non-dimensional spanwise unit = $y/_{\frac{b}{2}}$.
ρ	Standard air density.
ϕ	Velocity potential.
$\phi_{c/4}$	Angle of sweep of the quarter chord-line.
$\phi_{c/2}$	Angle of sweep of the mid-chord line.
$\bar{}$	barred values are in the transformed plane.

Suffices:-

US	upper surface.
LS	lower surface.
W	wing.
B	body.
T	Trefftz-plane.

THE LIFT DISTRIBUTION AND THE LIFT CURVE SLOPE FOR WING/BODY COMBINATIONS

1. INTRODUCTION

1.1 Early investigations into the aerodynamic forces acting on wing/body combinations were carried out simply by adding, algebraically, the forces on the wing alone to those on the body. In 1927[1] however, it was pointed out that the total drag of an aircraft was considerably different from the value calculated by adding the skin friction drag of each component and the induced drag of the whole due to lift, and it was realised that some factor was being ignored by this method. As the design of the individual components improved, this discrepancy became more pronounced and investigations into this mutual interference effect were started. Since it is of importance to know the spanwise lift distribution over a wing/body combination in order to predict the structural loads to be expected upon it, studies were made of this interference as it effects the lifting forces on combinations of this nature.

Since aircraft specifications tend to seek greater and greater versatility - in particular, supersonic speed capabilities for undertaking some mission coupled with low speed manoeuvorability for take-off and landing -, an investigation into lift distribution must be applicable to many different wing planforms, especially the low aspect ratio, delta, or arrow-shaped wings which are being considered for so many supersonic aircraft.

A number of methods have been proposed for calculating this lift distribution, but each method imposes some rigid condition on the size and shape of the combination for which the method is valid.

An attempt is made in this paper to find the most versatile method of solving this problem for the low speed régime, assuming that the flow is incompressible and non-viscous.

The various theories put forward can be broadly divided into two groups:- those directly based on the Prandtl lifting line theory, and those which are not. For the case of wings alone, of aspect ratio of 5 or less, the Prandtl theory predicts a lift curve slope appreciably higher than the correct value, and it is reasonable to suppose that this will also be the case for wing/body combinations of aspect ratio 5 or less. Hence the first group of theories breaks down for these small aspect ratios.

1.2 The first investigation - based on lifting line theory - was by Lennertz[2] who considered an infinitely long circular cylindrical body in combination with a rectangular wing of high aspect ratio: this theory was generalised by Pepper[3] to include infinitely long bodies of any cross-sectional shape. Multhopp[4], in his method also based on lifting line theory, considered a high aspect ratio wing on an infinitely long cylinder of any cross-section and he also suggested corrections to allow for a non-cylindrical finite body.

In the second group of methods, Zlotnick and Robinson[5] proposed a method for circular bodies in which they represented the wing lifting elements by horse-shoe vortices. Slender-winged bodies of revolution which have wings with straight trailing edges are dealt with by Spreiter[6], using a method which is based on the theory of Jones[7] although this is only strictly correct for wings of zero aspect ratio. For low aspect ratio wing/body combinations which are rather more than slender, Lawrence[8] has given a solution which has been generalised[9] to cover the case of cylindrical bodies of any cross-sectional shape.

In chapter 2 of this paper there is a brief summary of the methods used by Lennertz, Multhopp, Spreiter, and Luckert, and in chapter 3 a detailed account is given of Multhopp's method with the extensions suggested by Weber, Kirby, and Kettle. This seems to be the most versatile method of tackling the wing/body problem as the extensions allow for wing thickness, taper, and sweep-back. Chapter 4 gives a brief account of the numerical procedure, using a DEUCE computer, adopted to deal with the theory of chapter 3. Some experimental considerations are also included in this chapter. An analysis of the results, both theoretical and experimental, is given in chapter 5, and comparisons and conclusions appear in chapter 6.

2. SUMMARY OF METHODS.

2.1 Lennertz[2] considered infinitely long circular cylindrical bodies in combination with wings, and he used the Prandtl wing-theory.

In the Trefftz plane - i.e. the plane so far downstream that the stream can be taken as extending to infinity both upstream and downstream, - the free vortices from the trailing edge of the wing area induce a flow about the body section and the lift is given as the impulse per unit time of this stream (or the rate of change of vertical momentum). Thus:

$$L = -\rho V_0 \iint \frac{\partial \phi}{\partial z} \, dy \, dz \qquad \text{-------(2.1)}$$

this being evaluated over the entire plane outside the body and vortex band cross-section.

For the case of uniform spanwise lift distribution an expression for ϕ can be obtained by the use of images of the free vortices relative to the body surface - the free vortices being liberated only at the ends of the wing. Integration with respect to z can then be carried out to give the spanwise lift distribution: integration with respect to y then gives a value for the total lift.

Expression (2.1) can be transformed into a line integral by means of Stokes Theorem and the field of integration can be changed to that denoted by $\int_R^{\frac{b}{2}}$, where b is the wing span and R is the body radius: the following expression is then obtained:

$$L = 2\rho V_o \int_R^{\frac{b}{2}} \Gamma(y)\left(1 + \frac{R^2}{y^2}\right) dy \qquad \text{------(2.2)}$$

Lennertz then introduces conditions which hold in the case of minimum induced drag and he obtains expressions for the circulation and lift over the wing area and the lift distribution over the body width.

For the case of minimum induced drag he obtains:

$$\frac{L_w'}{\rho V_o} = \Gamma(y) = \Gamma_m \cdot \frac{\left(\frac{b}{2}\right)^2 + R^2}{\left(\frac{b}{2}\right)^2 - R^2} \cdot \sqrt{1 - \frac{\left(\frac{b}{2}\right)^2}{\left[\left(\frac{b}{2}\right)^2 + R^2\right]^2} \cdot \frac{\left(y^2 + R^2\right)^2}{y^2}} \qquad \text{------(2.3)}$$

and

$$\frac{L_B'}{\rho V_o} = \Gamma_m \cdot \frac{b}{\left(\frac{b}{2}\right)^2 - R^2} \cdot \left[\sqrt{\frac{\left[\left(\frac{b}{2}\right)^2 + R^2\right]^2}{b^2} - y^2} - \sqrt{R^2 - y^2}\right] \qquad \text{------(2.4)}$$

where L_w' is the lift distribution over the wing area;

L_B' is the lift distribution over the body width;

and Γ_m is the circulation at the wing/body junction.

also $$L' = \frac{1}{2} \rho V_o^2 c\, C_L \qquad \text{------(2.5)}$$

$$\therefore \quad \frac{L'}{\rho V_o} = \frac{b\, V_o\, c\, C_L}{2b} \qquad \text{------(2.6)}$$

Now introduce non-dimensional circulation given by

$$\gamma(y) = \frac{\Gamma(y)}{b V_o} \qquad \text{------(2.7)}$$

and non-dimensional units of length

$$\eta = \frac{y}{b/2} \qquad \text{-------(2.8)}$$

and equations (2.3) and (2.4) become:

$$\frac{C_L(\eta)\cdot c}{2b} = \gamma(\eta) = \gamma_{root} \times \frac{1+\left(\frac{D}{b}\right)^2}{1-\left(\frac{D}{b}\right)^2}\sqrt{1-\frac{1}{\left[1+\left(\frac{D}{b}\right)^2\right]^2}\frac{\left[\eta^2+\left(\frac{D}{b}\right)^2\right]^2}{\eta^2}} \qquad \text{---(2.9)}$$

for $\frac{D}{b} \leq |\eta| \leq 1$

and

$$\frac{C_L(\eta)\cdot c}{2b} = \gamma_{root} \times \frac{2}{1-\left(\frac{D}{b}\right)^2}\left[\sqrt{\frac{\left[1+\left(\frac{D}{b}\right)^2\right]^2}{4}-\eta^2} - \sqrt{\left(\frac{D}{b}\right)^2-\eta^2}\right] \qquad \text{---(2.10)}$$

for $0 \leq |\eta| \leq \frac{D}{b}$

2.2 The method proposed by Multhopp[4] for dealing with the wing/body problem obviates the necessity of introducing the images of the vortices in the body surface as done by Lennertz.

A rectangular co-ordinate system of axes is used, in which the yz-plane is normal to the axis of the fuselage, and the z-axis is vertically downwards.

Multhopp applies a conformal transformation to the flow normal to the fuselage so that the fuselage cross-section becomes a vertical slit. Most fuselage cross-sections can be transformed into a circle or ellipse, so he starts with the assumption of a circular cross-section.

Let $u = z + iy$ ----------(2.11)

be the complex variable in the plane vertical to the fuselage axis, and

$\bar{u} = \bar{z} + i\bar{y}$ ----------(2.12)

be the complex variable in the transformed plane.

If the body is at incidence α_B to the main flow, then the y-component of the additional downwash produced by the isolated body is given by (see appendix 1):

$$v_{y_B} = -\alpha_B V_0 \left[\mathcal{R}\left(\frac{d\bar{u}}{du}\right) - 1 \right] \quad \text{-----(2.13)}$$

where $\mathcal{R}\left(\frac{d\bar{u}}{du}\right)$ is the real part of the differential quotient $\left(\frac{d\bar{u}}{du}\right)$, and the negative sign indicates that it is actually an upwash.

The normal downward velocity can be split into three quantities:-

$$v_z = -\alpha_w V_o + v_{z_B} + v_{z_i} \qquad \text{------(2.14)}$$

where α_w is the local angle of incidence of the wing section;

v_{z_B} is the additional downward velocity due to the effect of the body;

and v_{z_i} is the induced velocity due to the trailing vortices.

The induced velocity at the wing in the transformed plane is given by

$$\bar{v}_{z_i}(\bar{y}) = \frac{1}{4\pi}\int_{-\frac{\bar{b}}{2}}^{+\frac{\bar{b}}{2}} \frac{d\Gamma}{d\bar{y}'}\,\frac{d\bar{y}'}{\bar{y}-\bar{y}'} \qquad \text{------(2.15)}$$

and by multiplying this by $\mathcal{R}\left(\frac{d\bar{u}}{du}\right)$ Multhopp obtains the induced velocity at the wing in the original plane:

$$v_{z_i}(y) = \mathcal{R}\left(\frac{d\bar{u}}{du}\right)\frac{1}{4\pi}\int_{-\frac{\bar{b}}{2}}^{+\frac{\bar{b}}{2}} \frac{d\Gamma}{d\bar{y}'}\,\frac{d\bar{y}'}{\bar{y}-\bar{y}'} \qquad \text{------(2.16)}$$

He now considers the circulation around a wing section of unit span.

$$\Gamma = \frac{1}{2}\, c\, V_o\, \frac{dC_L}{d\alpha}\cdot\alpha_{eff} \qquad \text{------(2.17)}$$

where α_{eff} is the angle between the local direction of flow and the direction of zero lift of the wing section.

Also $$\alpha_{eff} = -\frac{v_z}{V_o} \qquad \text{------(2.18)}$$

where v_z is the flow component normal to the direction of zero lift.

Denoting $\frac{dC_L}{d\alpha}$ by a_0, equations (2.14), (2.17), and (2.18) give :-

$$\Gamma = -\frac{1}{2} c v_z a_0 \qquad \text{------(2.19)}$$

$$= \frac{1}{2} c a_0 \left[\alpha_w V_0 - v_{\gamma_B} - v_{\gamma_i} \right] \qquad \text{------(2.20)}$$

Thus from equations (2.EE), (2.16), and (2.20) ,

$$\Gamma(\bar{y}) = \frac{1}{2} a_0 c(\bar{y}) \left\{ \alpha_w(\bar{y}) V_0 + \alpha_B V_0 \left[R\left(\frac{d\bar{u}}{du}\right) - 1 \right] - R\left(\frac{d\bar{u}}{du}\right) \frac{1}{4\pi} \int_{-\frac{b}{2}}^{\frac{b}{2}} \frac{d\Gamma}{d\bar{y}'} \cdot \frac{d\bar{y}'}{\bar{y} - \bar{y}'} \right\} \qquad \text{---(2.21)}$$

Multhopp now introduces non-dimensional circulation, $\bar{\gamma}$, and spanwise co-ordinate, $\bar{\eta}$, given by :-

$$\bar{\gamma} = \frac{\Gamma}{\bar{b} V_0} \quad \text{and} \quad \bar{\eta} = \bar{y} \big/ \tfrac{b}{2} \qquad \text{-----(2.22)}$$

and he forms

$$\bar{\alpha}_i = \frac{1}{2\pi} \int_{-1}^{+1} \frac{d\bar{\gamma}}{d\bar{\eta}'} \cdot \frac{d\bar{\eta}'}{\bar{\eta} - \bar{\eta}'} \qquad \text{----(2.23)}$$

From equations (2.21), (2.22), and (2.23) he obtains:

$$\bar{\gamma}(\bar{\eta}) = \frac{a_0 c(\bar{\eta})}{2\bar{b}} R\left(\frac{d\bar{u}}{du}\right) \left\{ \frac{\alpha_w(\bar{\eta}) - \alpha_B}{R\left(\frac{d\bar{u}}{du}\right)} + \alpha_B - \bar{\alpha}_i(\bar{\eta}) \right\} \qquad \text{------(2.24)}$$

He next splits this distribution into two components, $\bar{\gamma}_0$ being the distribution due to the geometric incidence $(\alpha_w - \alpha_B)$ and the induced downwash associated with it, and $\bar{\gamma}_B$ that due to the additional body upwash at the wing and also to the induced downwash daused by the body.

Thus $\quad \bar{\gamma}(\bar{\eta}) = \bar{\gamma}_0(\bar{\eta}) + \bar{\gamma}_B(\bar{\eta}) \qquad$ -----(2.25)

Hence $\bar{\gamma}_0(\bar{\eta}) = \frac{a_0 c(\bar{\eta})}{2\bar{b}} R\left(\frac{d\bar{u}}{du}\right)\left\{\frac{\alpha_w(\bar{\eta})-\alpha_B}{R\left(\frac{d\bar{u}}{du}\right)} - \bar{\alpha}_{i_0}(\bar{\eta})\right\}$ ---(2.26)

and $\bar{\gamma}_B(\bar{\eta}) = \frac{a_0 c(\bar{\eta})}{2\bar{b}} R\left(\frac{d\bar{u}}{du}\right)\left\{\alpha_B - \bar{\alpha}_{i_B}(\bar{\eta})\right\}$ ---(2.27)

where $\bar{\alpha}_i(\bar{\eta}) = \bar{\alpha}_{i_0}(\bar{\eta}) + \bar{\alpha}_{i_B}(\bar{\eta})$ ---(2.28)

Multhopp then goes on to consider the distribution over the breadth of the fuselage. To do this, he first shows that this distribution is similar to the variation of potential ϕ over the breadth.

This is done by applying Bernoulli's Theorem:

$$p_0 + \tfrac{1}{2}\rho V_0^2 = p + \tfrac{1}{2}\rho\left[(V_0 + v_x)^2 + (v_y)^2 + (v_z)^2\right] \qquad \text{---(2.29)}$$

Neglecting second order terms, this becomes :-

$$p - p_0 = -\rho V_0 v_x = -\rho V_0 \frac{\partial\phi}{\partial x} \qquad \text{---(2.30)}$$

Integrating this equation over an infinitely long strip of the fuselage gives :-

$$\int_{-\infty}^{+\infty} (p - p_0)\, dx = -\rho V_0 \phi(\infty) \qquad \text{---(2.31)}$$

since $\phi(-\infty) = 0$

The left side of equation (2.31), when taken over both the upper and lower surfaces of the body, is a measure of the lift experienced by the strip under consideration, and hence the lift at any strip is directly dependent on the value of ϕ in the Trefftz plane.

In the $\bar{u}$ -plane, with the fuselage being represented by a vertical slit, there are no singularities outside the wing and so $\phi(\bar{z})$ can be expanded into a power series with respect to $(\bar{z}-\bar{z}_w)$:-

$$\phi(\bar{z}) = \phi(\bar{z}_w) + (\bar{z}-\bar{z}_w)\cdot\frac{\partial\phi}{\partial\bar{z}}(\bar{z}_w) + \frac{(\bar{z}-\bar{z}_w)^2}{2}\cdot\frac{\partial^2\phi}{\partial\bar{z}^2}(\bar{z}_w) + \cdots \quad \text{---}(2.32)$$

Multhopp only considers the first two terms of this series.

Now for $\bar{z} < \bar{z}_w$, $\quad \phi(\bar{z}_w) = -\frac{\Gamma}{2}(\bar{y}=0) \quad$ ---(2.33)

while for $\bar{z} > \bar{z}_w$, $\quad \phi(\bar{z}_w) = +\frac{\Gamma}{2}(\bar{y}=0) \quad$ ---(2.34)

Hence $\quad \phi_{us}(\bar{z}_w) - \phi_{ls}(\bar{z}_w) = \Gamma \quad$ ---(2.35)

where $_{us}$ and $_{ls}$ denote upper and lower surfaces respectively.

Also $\quad \frac{\partial\phi}{\partial\bar{z}}(\bar{z}_w) = \bar{v}_{\gamma i_T}(\bar{y}=0) \quad$ ---(2.36)

where $\bar{v}_{\gamma i_T}$ is the induced downwash in the transformed Trefftz plane.

Thus from equations (2.32), (2.35), and (2.36) an expression for $\left[\phi_{us}(\bar{z}) - \phi_{ls}(\bar{z})\right]$ can be obtained for varying values of $\bar{z}$ and hence of $\bar{y}$. Using equation (2.31) now gives a measure of the lift.

2.3 The work done by Spreiter[6] on wing/body combinations is based on assumptions used by Munk[10] in his slender airship theory, and on the low aspect ratio pointed-wing theory developed by Jones[7] from Munk's work.

He approximates the flow around the combination by considering it to be two dimensional in planes perpendicular to the fuselage axis. Thus the flow in each such transverse plane is independent of that in adjacent planes. Considering an arbitrary transverse plane, $x = x_0$, fixed in space, during the passage of the wing/body combination the flow pattern is approximately similar to that of the transverse flow around an infinite cylinder of cross-section similar to that of the combination at the section $x = x_0$.

Spreiter then goes on to obtain the velocity potential for this flow.

By means of the Joukowski transformation, the cylinder with cross-section similar to that of the wing/body combination (circular body cross-section with flat plate wings diametrically opposed to each other) can be mapped conformally into a flat plate of infinite length. Considering the fuselage and wing to be in the X-plane and the transformation in the ζ-plane, the complex potential around the infinitely long flat plate is [11]

$$w' = \phi' + i\psi' = -i V_0 \alpha \sqrt{\zeta^2 - d^2} \qquad \text{------(2.37)}$$

where d is the semi-span of the transformed flat plate, and the prime indicates values in the ζ -plane. Transforming back to the X -plane gives the complex potential to be

$$w = \phi + i\psi = -i V_0 \alpha \sqrt{\left(X + \frac{a^2}{X}\right)^2 - \left(s + \frac{a^2}{s}\right)^2} \qquad \text{------(2.38)}$$

where a is the radius of the body, and s is the wing semi-span of the combination.

If polar co-ordinates -- $X = r(\cos\theta + i\sin\theta)$ -- are now introduced, equation (2.38) gives:-

$$\phi = \pm \frac{V_0 \alpha}{\sqrt{2}} \sqrt{\sqrt{r^4\left(1+\frac{a^8}{r^8}\right) + 2a^4\cos 4\theta + s^4\left(1+\frac{a^4}{s^4}\right)^2 - 2s^2\left(1+\frac{a^4}{s^4}\right)\left(1+\frac{a^4}{r^4}\right)r^2\cos 2\theta} + \left[-\left(1+\frac{a^4}{r^4}\right)r^2\cos 2\theta + s^2\left(1+\frac{a^4}{s^4}\right)\right]} \qquad \text{------(2.39)}$$

Spreiter considers the body radius a and the wing semi-span s to be functions of time, and treats equation (2.39) as the velocity potential of the unsteady flow through the plane $x = x_0$.

For unsteady two-dimensional incompressible flow, the pressure at a point is [12] :-

$$-\frac{p}{\rho} = \frac{\partial\phi}{\partial t} + \frac{1}{2}(v^2 + w^2) + F(t) \qquad \text{------(2.40)}$$

Hence the differential pressure between two points symmetrically positioned above and below the wing/body surface at any instant is given by

$$\frac{\Delta p}{\rho} = 2\frac{\partial\phi_1}{\partial t} - \frac{1}{2}(v_2^2 + w_2^2) + \frac{1}{2}(v_1^2 + w_1^2) \qquad \text{------(2.41)}$$

since $\dfrac{\partial \phi_2}{\partial t} = -\dfrac{\partial \phi_1}{\partial t}$ due to symmetry, where the subscript $_1$ denotes the point above the wing/body surface, and $_2$ denotes the point below it.

On the wing/body surface

$$v_1^2 + w_1^2 = v_2^2 + w_2^2$$

and hence
$$\frac{\Delta p}{\rho} = 2\,\frac{\partial \phi_1}{\partial t} \qquad \text{------(2.42)}$$

Also
$$\frac{\partial \phi_1}{\partial t} = \frac{\partial \phi_1}{\partial x}\cdot\frac{dx}{dt} = \frac{\partial \phi_1}{\partial x}\cdot V_0 \qquad \text{------(2.43)}$$

$$\frac{\Delta p}{q} = \frac{4\,\dfrac{\partial \phi_1}{\partial x}}{V_0} = \frac{4}{V_0}\left(\frac{\partial \phi_1}{\partial s}\cdot\frac{ds}{dx} + \frac{\partial \phi_1}{\partial a}\cdot\frac{da}{dx}\right) \qquad \text{------(2.44)}$$

Substituting the value of ϕ from equation (2.39), letting $\theta = 0$ or π for the wing loading and $r = a$ for the fuselage loading, and converting back to cartesian co-ordinates for the fuselage loading gives :-

$$\left(\frac{\Delta p}{q}\right)_W = 4\alpha\left\{\frac{\dfrac{ds}{dx}\left(1-\dfrac{a^4}{s^4}\right) + \dfrac{da}{dx}\left[2\dfrac{a}{s}\left(\dfrac{a^2}{s^2} - \dfrac{a^2}{r^2}\right)\right]}{\sqrt{\left(1+\dfrac{a^4}{s^4}\right) - \dfrac{r^2}{s^2}\left(1+\dfrac{a^4}{r^4}\right)}}\right\} \qquad \text{---(2.45)}$$
$$a \leq r \leq s$$

$$\left(\frac{\Delta p}{q}\right)_B = 4\alpha\left\{\frac{\dfrac{ds}{dx}\left(1-\dfrac{a^4}{s^4}\right) + 2\dfrac{a}{s}\,\dfrac{da}{dx}\left(1+\dfrac{a^2}{s^2} - 2\,\dfrac{y^2}{a^2}\right)}{\sqrt{\left(1+\dfrac{a^2}{s^2}\right)^2 - 4\,y^2/s^2}}\right\} \qquad \text{---(2.46)}$$
$$0 \leq y \leq a$$

The loading over the wing is thus given by equation (2.45), and that over the breadth of the fuselage by equation (2.46).

2.4 In the paper prepared by H.J.Luckert[13], the author approaches the problem by means of a simple analogy. He points out that equation (2.24) has the exact form of the equation for the circulation of a wing alone, whose chord is the chord of the original wing multiplied by the factor $R\left(\frac{d\bar{u}}{du}\right)$, and whose wing-setting is the original value divided by this same factor.

Equation (2.24) can be re-written in a different form:

$$\mathcal{P}(\bar{\gamma}\,;\bar{p}) = \alpha_B + \frac{\alpha_w - \alpha_B}{R\left(\frac{d\bar{u}}{du}\right)} \qquad \text{------(2.47)}$$

where:

$$\mathcal{P}(\bar{\gamma}\,;\bar{p}) = \bar{\alpha}_i(\bar{\eta}) + \bar{p}\,\bar{\gamma}(\bar{\eta}) \qquad \text{------(2.48)}$$

and

$$\bar{p} = \frac{2\bar{b}}{a_0\, c(\bar{\eta})} \cdot \frac{1}{R\left(\frac{d\bar{u}}{du}\right)} \qquad \text{------(2.49)}$$

Luckert then introduces the mathematical process known as the Weissinger[14] L-Method, and by analogy, the equation for lift distribution is written as:

$$\mathcal{L}(\bar{\gamma}\,;\bar{\lambda}) = \alpha_B + \frac{\alpha_w - \alpha_B}{R\left(\frac{d\bar{u}}{du}\right)} \qquad \text{------(2.50)}$$

where

$$\mathcal{L}(\bar{\gamma}\,;\bar{\lambda}) = \frac{1}{\pi}\int_{-1}^{+1} \frac{d\bar{\gamma}}{d\bar{\eta}'} \cdot \frac{d\bar{\eta}'}{\bar{\eta}-\bar{\eta}'} + \frac{\bar{\lambda}}{2\pi}\int_{-1}^{+1} \frac{d\bar{\gamma}}{d\bar{\eta}'} \cdot L\left[\bar{\lambda}(\bar{\eta}-\bar{\eta}')\right] d\bar{\eta}' \qquad \text{---(2.51)}$$

with

$$\bar{\lambda} = \frac{\bar{b}}{c(\bar{\eta}) \cdot R\left(\frac{d\bar{u}}{du}\right)} \qquad \text{------(2.52)}$$

and

$$L\left[\bar{\lambda}(\bar{\eta}-\bar{\eta}')\right] = \frac{\sqrt{1 + \bar{\lambda}^2(\bar{\eta}-\bar{\eta}')^2} - 1}{\bar{\lambda}(\bar{\eta}-\bar{\eta}')} \qquad \text{------(2.53)}$$

De Young and Harper[15] give a method for solving equation (2.50).

3. THE LOAD DISTRIBUTION OVER A WING/BODY COMBINATION.

3.1 The theoretical approach adopted in this paper is based on the method used by Multhopp[4] and the extensions suggested by Weber, Kirby, and Kettle[16].

Let x, y, z be a system of rectangular co-ordinate axes with the x-axis in the direction of the main stream flow, the z-axis vertically downwards, and the y-axis mutually perpendicular as shown in figure 1. Consider a wing/body combination consisting of wings of any planform mounted centrally on a long fuselage which is of the form of a circular cylinder at that section at which the wings are positioned. Consider this combination at incidence in a uniform flow of velocity V_0.

As seen in figure 2, the upwash due to the body is $V_0\alpha_B$ (considering only first order terms). Now this upwash is displaced by the body and thus causes additional upwash at the wing/body junction and on the wing near this junction. This additional upwash on the wing will produce a certain amount of lift even when the wing is at zero angle of incidence.

The load distribution over the combination must be such that the downwash induced by it, together with the free stream, have no components of velocity perpendicular to the surfaces of the wing and body.

If the assumption is made -as in linearised theory-that the wake is in the direction of the undisturbed free stream flow, the load distribution can be obtained by considering the section of the wake in the Trefftz-plane --i.e., in a plane far enough downstream to be able to ignore the effects of the bound vortices--which is equal to the actual section of the wing/body combination. By making this section a streamline in a flow upwards in this plane, the circulation, and hence the load distribution corresponding to minimum induced drag can be found.

The cross-section of the combination in the Trefftz-plane can be conformally transformed into a configuration with the body represented by a vertical slit in the line of symmetry, and this is then a stream-line in upward flow. Since the transformation is conformal, the potential, and hence the circulation, are unaffected by it. Of course the downwash due to the trailing vortices will not have the same value at the wing/body combination as it has in the Trefftz-plane, and it will be necessary to consider corrected values for this downwash.

The value usually taken for the induced downwash at the wing is half its value in the Trefftz-plane and this is here considered to be the case for that part of the downwash due to the wings. However, for the additional downwash due to the presence of the body a different value is used. In general, the root chord is greater than the body diameter, and that part of the wing covered by the fuselage can be considered as a twisted wing of small aspect ratio. For a small aspect ratio wing, the induced downwash at the wing is equal to that in the Trefftz-plane[17], and hence that is the value used here.

3.2 The lift distribution over the wing is given by:-

$$C_L(y) = \left(\frac{dC_L}{d\alpha_{eff}}\right)_y \cdot \alpha_{eff}(y) = a(y) \cdot \alpha_{eff}(y) \qquad \text{------(3.1)}$$

where $a(y)$ is the sectional lift curve slope. The effective incidence, α_{eff}, depends upon the total upward velocity component of the main flow V_0:

$$\alpha_{eff} = -\frac{v_z}{V_0} \qquad \text{------(3.2)}$$

where v_z is the velocity component in the direction of the z-axis, i.e. downwards. This component, or downwash, can be split into three terms, viz:-

$$v_z = -V_0\alpha_w + v_{z_B} + v_{z_i} \qquad \text{------(3.3)}$$

where v_{z_B} is the downwash (negative, since it is actually an upwash) produced by the body as previously explained, and v_{z_i} is the induced downwash due to the trailing vortices.

The assumption is now made that the cross-section of the combination in the Trefftz-plane is given by the complex variable

$$u = z + iy \qquad \text{------(3.4)}$$

while the complex variable in the transformed plane is

$$\bar{u} = \bar{z} + i\bar{y} \qquad \text{------(3.5)}$$

where $\bar{u}$ is a function of u so that the body cross-section is transformed into a vertical slit.

Now in the u-plane the main flow has a velocity equal to $-\alpha_B V_0$ in the z-direction, causing a downwash due to the body given by (see appendix 1)

$$v_{\gamma_B} = -V_o \alpha_B \left[R\left(\frac{d\bar{u}}{du}\right) - 1 \right] \qquad \text{------(3.6)}$$

The circulation is unaltered by the transformation, and so the induced velocity at a point $\bar{y}$ in the transformed Trefftz-plane is given by

$$\bar{v}_{\gamma_i}(\bar{y})_T = \frac{1}{2\pi} \int_{-\frac{\bar{b}}{2}}^{+\frac{\bar{b}}{2}} \frac{d\Gamma}{d\bar{y}'} \cdot \frac{d\bar{y}'}{\bar{y} - \bar{y}'} \qquad \text{------(3.7)}$$

which gives, in the u -plane

$$v_{\gamma_i}(y)_T = \frac{1}{2\pi} R\left(\frac{d\bar{u}}{du}\right) \int_{-\frac{\bar{b}}{2}}^{+\frac{\bar{b}}{2}} \frac{d\Gamma}{d\bar{y}'} \cdot \frac{d\bar{y}'}{\bar{y} - \bar{y}'} \qquad \text{------(3.8)}$$

Non-dimensional units are introduced for the circulation and the spanwise co-ordinate:

$$\gamma(y) = \frac{\Gamma(y)}{b V_o} \; ; \; \bar{\gamma}(\bar{y}) = \frac{\Gamma(\bar{y})}{\bar{b} V_o} = \frac{b}{\bar{b}} \gamma(y) \qquad \text{------(3.9)}$$

and

$$\bar{\eta} = \bar{y} / \tfrac{\bar{b}}{2} \qquad \text{------(3.10)}$$

thus making equation (3.8) become

$$v_{\gamma_{i_T}} = R\left(\frac{d\bar{u}}{du}\right) \cdot \frac{V_o}{\pi} \int_{-1}^{1} \frac{d\bar{\gamma}}{d\bar{\eta}'} \cdot \frac{d\bar{\eta}'}{\bar{\eta} - \bar{\eta}'} \qquad \text{------(3.11)}$$

Now, from the Kutta-Joukowski Theorem,

$$\Gamma(y) = \frac{1}{2} V_o \, c(y) \, C_L(y) \qquad \text{------(3.12)}$$

and so, from equations (3.9), (3.12), and (3.1), an expression for $\gamma(y)$ is obtained:

$$\gamma(y) = \frac{C_L(y) \cdot c(y)}{2b} = \frac{a(y) \cdot c(y)}{2b} \cdot \alpha_{eff}(y) \qquad \text{------(3.13)}$$

The effect of taper can now be allowed for by means of the $c(y)$ term which can vary as y varies over the span.

From equations (3.2), (3.3), and (3.6),

$$\gamma(y) = \frac{a.\,c(y)}{2b}\left\{\alpha_w(y) + \alpha_B(y)\left[R\left(\frac{d\bar{u}}{du}\right) - 1\right] - \frac{v_{\gamma_i}(y)}{V_0}\right\} \quad \text{-----}(3.14)$$

or, from equation (3.9),

$$\bar{\gamma}(\bar{\eta}) = \frac{a.\,c(\bar{\eta})}{2\bar{b}}\left\{\alpha_w(\bar{\eta}) + \alpha_B(\bar{\eta})\left[R\left(\frac{d\bar{u}}{du}\right) - 1\right] - \frac{v_{\gamma_i}(\bar{\eta})}{V_0}\right\} \quad \text{-----}(3.15)$$

To allow for the two different values used for the downwash at the wing/body combination, as explained in section 3.1, it is necessary to split the last term on the right side of equation (3.15) into two parts:

$$v_{\gamma_i} = v_{\gamma_{i_W}} + v_{\gamma_{i_B}} \quad \text{------}(3.16)$$

where $v_{\gamma_{i_W}} = \frac{1}{2} v_{\gamma_{i_T}}$ ------(3.17)

and $v_{\gamma_{i_B}} = v_{\gamma_{i_T}}$ ------(3.18)

Thus equation (3.15) becomes:-

$$\bar{\gamma}(\bar{\eta}) = \frac{a.\,c(\bar{\eta})}{2\bar{b}}\left\{\alpha_w(\bar{\eta}) + \alpha_B(\bar{\eta})\left[R\left(\frac{d\bar{u}}{du}\right) - 1\right] - \frac{1}{2\pi}R\left(\frac{d\bar{u}}{du}\right)\int_{-1}^{1}\frac{d\bar{\gamma}_W(\bar{\eta}')}{d\bar{\eta}'}\cdot\frac{d\bar{\eta}'}{\bar{\eta}-\bar{\eta}'}\right.$$

$$\left. - \frac{1}{\pi}R\left(\frac{d\bar{u}}{du}\right)\int_{-1}^{1}\frac{d\bar{\gamma}_B(\bar{\eta}')}{d\bar{\eta}'}\cdot\frac{d\bar{\eta}'}{\bar{\eta}-\bar{\eta}'}\right\} \quad \text{-----}(3.19)$$

where $\bar{\gamma}_W(\bar{\eta}')$ depends on α_w and not on α_B,

and $\bar{\gamma}_B(\bar{\eta}')$ depends on α_B and not on α_w.

3.3 Consider now the extensions to this basic method to allow for the effects of sweep-back and of finite wing thickness.

For the unswept flat wing the value of the lift curve slope, a, is constant along the span. However, in the case of a swept wing, with or without a body, the chordwise loading is altered at the wing/body junction or at the centre section, and thus the sectional lift slope varies over this region.

Küchemann[18] gives two expressions for $a(y)$, the relevant one being decided by the position of the section under consideration.

$$a(y) = a_s - \frac{\Delta\lambda(y)}{\Delta\lambda_c}\left[a_s - a_c\right] \qquad \text{------(3.20)}$$

$$a(y') = a_s + \frac{\Delta\lambda(y')}{\Delta\lambda_c}\left[a_T - a_s\right] \qquad \text{------(3.21)}$$

where y is the distance of the section from the centre-line;

y' is the distance of the section from the tip;

a_c is the lift curve slope at the centre section;

a_T is the lift curve slope at the tip;

and a_s is the lift curve slope for an infinite sheared wing.

a_s, a_c, and a_T are given by

$$a_s = a_0 \cos\phi_{c/4} \qquad \text{------(3.22)}$$

$$a_c = a_0\left(1 - \frac{\phi_{c/2}}{\frac{\pi}{2}}\right) \qquad \text{------(3.23)}$$

$$a_T = a_0\left(1 + \frac{\phi_{c/2}}{\frac{\pi}{2}}\right) \qquad \text{------(3.24)}$$

The displacement of the local aerodynamic centre, for the centre section of a swept wing, is given by[18]

$$\frac{\Delta h_c}{c} = \frac{\phi}{2\pi} \qquad \text{------(3.25)}$$

Thus $\dfrac{\Delta h(y)}{\Delta h_c} = \dfrac{\Delta h(y)}{c} \div \dfrac{\phi}{2\pi}$ ------(3.26)

and the graph of figure 3 gives the value of this expression for values of $\frac{y}{c}$ or $\frac{y'}{c}$.

As can be seen from this figure, the value of $\frac{\Delta h(y)}{\Delta h_c}$ becomes negligible for values of $\frac{y}{c}$ greater than about 0.9. Thus for

$$0 < \frac{y}{c} < 0.9 \qquad \text{and} \qquad \frac{y'}{c} > 0.9$$

the value of $a(y)$ in equation (3.20) is used; for $\frac{y}{c} > 0.9$ and $0 < \frac{y'}{c} < 0.9$ equation (3.21) is used. In the case of wings of small aspect ratio, it is possible for

$$0 < \frac{y}{c} < 0.9 \qquad \text{and} \qquad 0 < \frac{y'}{c} < 0.9$$

and the value of the lift curve slope is taken as the mean of the values given by equations (3.20) and (3.21). For a section at which both $\frac{y}{c}$ and $\frac{y'}{c}$ are greater than 0.9, such as around mid-semi-span af a large aspect ratio wing, the value of the lift curve slope is considered to be the same as that for an infinite sheared wing:

$$a(y) = a_s$$

Thus equation (3.19) becomes

$$\bar{\gamma}(\bar{\eta}) = \frac{a(\bar{\eta}).c(\bar{\eta})}{2\bar{b}}\left\{\alpha_w(\bar{\eta}) + \alpha_B(\bar{\eta})\left[R\left(\frac{d\bar{u}}{du}\right)-1\right] - \frac{1}{2\pi}R\left(\frac{d\bar{u}}{du}\right)\int_{-1}^{1}\frac{d\bar{\gamma}_w(\bar{\eta}')}{d\bar{\eta}'}.\frac{d\bar{\eta}'}{\bar{\eta}-\bar{\eta}'}\right.$$
$$\left. - \frac{1}{\pi}R\left(\frac{d\bar{u}}{du}\right)\int_{-1}^{1}\frac{d\bar{\gamma}_B(\bar{\eta}')}{d\bar{\eta}'}\frac{d\bar{\eta}'}{\bar{\eta}-\bar{\eta}'}\right\} \qquad \text{-----}(3.27)$$

The second extension to be considered is to make allowance for the effect of wing thickness. The main effect of finite thickness is to decrease the body upwash from the value it has when in combination with a thin wing. This is due to the fact that, if the wing and body are replaced by singularities, then only those singularities replacing the body outside the wing actually contribute to the upwash. To allow for this Weber, Kirby, and Kettle suggest decreasing the body upwash by a factor k which is taken as the ratio of the body cross-sectional area above and below the wing to the total cross-sectional area.

Thus, with wing thickness = t and body radius = R

$$k = 1 - \frac{2}{\pi}\sin^{-1}\frac{t}{2R} - \frac{2}{\pi}\frac{t}{2R}\sqrt{1-\left(\frac{t}{2R}\right)^2} \qquad \text{-----}(3.28)$$

and equation (3.6) becomes

$$v_{\gamma_B} = -\alpha_B V_0 k\left[R\left(\frac{d\bar{u}}{du}\right)-1\right] \qquad \text{------}(3.29)$$

For convenience, equation (3.29) can be written as

$$v_{\gamma_B} = -\alpha_B V_0\left[T(y) - 1\right] \qquad \text{------}(3.30)$$

by letting $T(y) = 1 + k\left[R\left(\frac{d\bar{u}}{du}\right)-1\right]$ ------(3.31)

Thus the effect of wing thickness is to alter the term $R\left(\frac{d\bar{u}}{du}\right)$ to $T(y)$.

Equation (3.27) now becomes

$$\bar{\gamma}(\bar{\eta}) = \frac{a(\bar{\eta}).c(\bar{\eta})}{2\bar{b}}\left\{\alpha_w(\bar{\eta}) + \alpha_B(\bar{\eta})\left[T(\bar{\eta}) - 1\right] - \frac{1}{2\pi}T(\bar{\eta})\int_{-1}^{1}\frac{d\bar{\gamma}_w(\bar{\eta}')}{d\bar{\eta}'}.\frac{d\bar{\eta}'}{\bar{\eta}-\bar{\eta}'}\right.$$
$$\left. - \frac{1}{\pi}T(\bar{\eta})\int_{-1}^{1}\frac{d\bar{\gamma}_B(\bar{\eta}')}{d\bar{\eta}'}.\frac{d\bar{\eta}'}{\bar{\eta}-\bar{\eta}'}\right\} \qquad \text{-----}(3.32)$$

The right side of this equation splits naturally into two parts, one dependent on α_w and the other on α_B : i.e. one part considering the wing incidence, together with the induced downwash caused by the wing, and a second part considering the total body upwash on the wing, together with the induced downwash caused by the body.

Thus equation (3.32) can be written as

$$\bar{\gamma}_w(\bar{\eta}) = \frac{a(\bar{\eta}).c(\bar{\eta})}{2\bar{b}}\left\{\alpha_w(\bar{\eta}) - \frac{1}{2\pi}T(\bar{\eta})\int_{-1}^{1}\frac{d\bar{\gamma}_w(\bar{\eta}')}{d\bar{\eta}'}.\frac{d\bar{\eta}'}{\bar{\eta}-\bar{\eta}'}\right\} \qquad \text{---}(3.33)$$

and $$\bar{\gamma}_B(\bar{\eta}) = \frac{a(\bar{\eta}).c(\bar{\eta})}{2\bar{b}}\left\{\alpha_B(\bar{\eta})\left[T(\bar{\eta}) - 1\right] - \frac{1}{\pi}T(\bar{\eta})\int_{-1}^{1}\frac{d\bar{\gamma}_B(\bar{\eta}')}{d\bar{\eta}'}.\frac{d\bar{\eta}'}{\bar{\eta}-\bar{\eta}'}\right\} \text{---}(3.34)$$

3.4 The load over the body can be determined by considering the difference of pressures between the upper and lower surfaces of the fuselage at a section in a plane parallel to the plane of symmetry.
This pressure difference can be given in terms of the potential function.

The total lift coefficient at the spanwise position is given by

$$C_L = \int_{-\infty}^{\infty} -\left(C_{p_{US}} - C_{p_{LS}}\right) d\left(\frac{x}{c}\right) \qquad \text{-----(3.35)}$$

where US and LS denote upper surface and lower surface respectively. Bernoulli's equation gives

$$p_0 + \frac{1}{2}\rho V_0^2 = p + \frac{1}{2}\rho V_0^2 \left\{\left(1+\frac{v_x}{V_0}\right)^2 + \left(\frac{v_y}{V_0}\right)^2 + \left(\frac{v_z}{V_0}\right)^2\right\} \qquad \text{---(3.36)}$$

$$\therefore\ c_p = \frac{p-p_0}{\frac{1}{2}\rho V_0^2} = -2\frac{v_x}{V_0} - \frac{v_x^2}{V_0^2} - \frac{v_y^2}{V_0^2} - \frac{v_z^2}{V_0^2} \qquad \text{---(3.37)}$$

$$\doteqdot -\frac{2}{V_0}\cdot\frac{\partial\phi}{\partial x} \qquad \text{---(3.38)}$$

to the first order.

Thus from equations (3.35) and (3.38)

$$C_L = \frac{2}{c V_0}\left[\left(\phi_{US}\right)_{-\infty}^{+\infty} - \left(\phi_{LS}\right)_{-\infty}^{+\infty}\right] \qquad \text{-----(3.39)}$$

$$= \frac{2}{c V_0}\left[\phi_{US}(x=\infty) - \phi_{LS}(x=\infty)\right] \qquad \text{-----(3.40)}$$

since $\phi_{US}(x=-\infty) = \phi_{LS}(x=-\infty) = 0$

Now, on the wing

$$\phi_{US}(\bar{z}_w) - \phi_{LS}(\bar{z}_w) = \Gamma \qquad \text{-----(3.41)}$$

where $\bar{z}_w$ corresponds to the z-coordinate of the junction; i.e. Γ is the value for the position $\bar{\eta} = 0$.

Also $$\left(\frac{\partial \phi}{\partial \bar{z}}\right)_{\bar{z}=\bar{z}_w} = \bar{v}_{z_{iT}}(\bar{z}_w) \qquad \text{------}(3.42)$$

$\phi(\bar{z})$ can be expanded into a Taylor series with respect to $(\bar{z}-\bar{z}_w)$,

$$\phi(\bar{z}) = \phi(\bar{z}_w) + \frac{\bar{z}-\bar{z}_w}{1!}\left(\frac{\partial \phi}{\partial \bar{z}}\right)_{\bar{z}=\bar{z}_w} + \frac{(\bar{z}-\bar{z}_w)^2}{2!}\left(\frac{\partial^2 \phi}{\partial \bar{z}^2}\right)_{\bar{z}=\bar{z}_w} + \cdots \qquad \text{---}(3.43)$$

From equations (3.40) and (3.43), taking the Taylor series to the second order,

$$C_L = \frac{2}{cV_0}\left[\left\{\phi_{US}(\bar{z}_w,\infty) - \phi_{LS}(\bar{z}_w,\infty)\right\} + \left(\frac{\partial \phi}{\partial \bar{z}}\right)_{\bar{z}=\bar{z}_w}\left\{(\bar{z}_{US}-\bar{z}_w) - (\bar{z}_{LS}-\bar{z}_w)\right\} + \frac{1}{2}\left(\frac{\partial^2 \phi}{\partial \bar{z}^2}\right)_{\bar{z}=\bar{z}_w}\left\{(\bar{z}_{US}-\bar{z}_w)^2 - (\bar{z}_{LS}-\bar{z}_w)^2\right\}\right] \qquad \text{------}(3.44)$$

Using equations (3.41) and (3.42), this can be written as

$$C_L = \frac{2}{cV_0}\left[\Gamma(\bar{\eta}=0) + \bar{v}_{z_{iT}}(\bar{z}_w)\cdot(\bar{z}_{US}-\bar{z}_{LS}) + \frac{1}{2}\left(\frac{\partial \bar{v}_{z_i}}{\partial \bar{z}}\right)_{\bar{z}=\bar{z}_w}\left\{(\bar{z}_{US}^2-\bar{z}_{LS}^2) - 2\bar{z}_w(\bar{z}_{US}-\bar{z}_{LS})\right\}\right]$$

$$= \frac{2}{cV_0}\left[\Gamma(\bar{\eta}=0) + (\bar{z}_{US}-\bar{z}_{LS})\left\{\bar{v}_{z_{iT}}(\bar{z}_w) + \frac{1}{2}\left(\frac{\partial \bar{v}_{z_i}}{\partial \bar{z}}\right)_{\bar{z}=\bar{z}_w}(\bar{z}_{US}+\bar{z}_{LS}-2\bar{z}_w)\right\}\right] \qquad \text{----}(3.45)$$

Hence: $$\gamma_{(y)} = \frac{C_L c}{2b}$$

$$= \gamma(\bar{\eta}=0) + \frac{(\bar{z}_{US}-\bar{z}_{LS})\left\{\bar{v}_{z_{iT}}(\bar{z}_w) + \frac{1}{2}\left(\frac{\partial \bar{v}_{z_i}}{\partial \bar{z}}\right)_{\bar{z}=\bar{z}_w}(\bar{z}_{US}+\bar{z}_{LS}-2\bar{z}_w)\right\}}{bV_0} \qquad \text{----}(3.46)$$

The overall lift distribution is now given by equations (3.33), (3.34), and (3.46): (3.33) and (3.34), when added together, give the distribution over the wing semi-span outside the body, and equation (3.46) gives the distribution over the semi-diameter of the body.

3.5 Consider now the case of a circular cylindrical body of radius R with a wing mounted in the mid-position as shown in figure 4, and consider also the transformed cross-section as shown in figure 5. The cross-section in figure 4 - the u-plane - is given by $u = z + iy$
and that in figure 5 - the $\bar{u}$-plane - is given by

$$\bar{u} = \bar{z} + i\bar{y}$$

For the circular body, the conformal transformation is given by Multhopp[4] as:

$$\bar{u} = u + \frac{R^2}{u} \qquad \text{------(3.47)}$$

$$\therefore \frac{d\bar{u}}{du} = 1 - \frac{R^2}{u^2} \qquad \text{------(3.48)}$$

$$= 1 - \frac{R^2(z - iy)^2}{(z^2 + y^2)^2} \qquad \text{------(3.49)}$$

$$\therefore \mathcal{R}\left(\frac{d\bar{u}}{du}\right) = 1 - \frac{R^2(z^2 - y^2)}{(z^2 + y^2)^2} \qquad \text{------(3.50)}$$

However, for the symmetrically placed wing, $z = 0$

$$\therefore \mathcal{R}\left(\frac{d\bar{u}}{du}\right) = 1 + \frac{R^2}{y^2} \qquad \text{------(3.51)}$$

From equation (3.31), allowing for wing thickness by altering $\mathcal{R}\left(\frac{d\bar{u}}{du}\right)$ to $T_{(y)}$,

$$T_{(y)} = 1 + k \cdot \frac{R^2}{y^2} \qquad \text{------(3.52)}$$

From the transformation

$$\bar{y} = y - \frac{R^2}{y} \qquad \text{------(3.53)}$$

the transformed semi-span is given by:

$$\frac{\bar{b}}{2} = \frac{b}{2} - \frac{R^2}{b/2}$$

$$= \frac{b}{2}\left[1 - \left(\frac{R}{b/2}\right)^2\right] \qquad \text{------(3.54)}$$

Hence $\bar{b} = b\left[1 - \left(\frac{R}{b/2}\right)^2\right]$ ------(3.55)

From equation (3.53)

$$y = \frac{\bar{y}}{2} + \sqrt{\left(\frac{\bar{y}}{2}\right)^2 + R^2} \qquad \text{------(3.56)}$$

also $\eta = \frac{y}{b/2}$ and $\bar{\eta} = \frac{\bar{y}}{\bar{b}/2}$ ------(3.57)

$$\therefore \quad \eta\frac{b}{2} = \frac{\bar{\eta}\bar{b}}{4} + \sqrt{\left(\frac{\bar{\eta}\bar{b}}{4}\right)^2 + R^2} \qquad \text{------(3.58)}$$

$$\therefore \quad \eta = \frac{1}{2}\bar{\eta}\frac{\bar{b}}{b} + \sqrt{\left(\frac{1}{2}\bar{\eta}\frac{\bar{b}}{b}\right)^2 + \left(\frac{R}{\bar{b}/2}\right)^2} \qquad \text{------(3.59)}$$

From equation (3.52)

$$T(\eta) = 1 + k\cdot\frac{R^2}{(\eta\cdot\frac{b}{2})^2}$$

$$= 1 + k\cdot\left(\frac{R}{b/2}\right)^2\cdot\frac{1}{\eta^2} \qquad \text{------(3.60)}$$

and also $T(\bar{\eta}) = 1 + k\left(\frac{R}{\bar{b}/2}\right)^2\cdot\frac{1}{\eta_T^2}$ ------(3.61)

where η_T is the value of η in the Trefftz-plane corresponding to the value $\bar{\eta}$ in the transformed plane, and is given by equation (3.59).

3.6 It is now possible to solve equations (3.33) and (3.34) using the quadrature formula developed by Multhopp[19] for unswept wings. In this method, the integral equations are replaced by a system of linear equations:-

$$\left(b_{\nu\nu} + \frac{2\bar{b}}{a(\bar{\eta}_\nu)\cdot c(\bar{\eta}_\nu)\cdot T(\bar{\eta}_\nu)}\right)\bar{\gamma}_w(\bar{\eta}_\nu) = \frac{\alpha_w(\bar{\eta}_\nu)}{T(\bar{\eta}_\nu)} + \sum_{n=1}^{m}{}' b_{\nu n}\bar{\gamma}_w(\bar{\eta}_n) \quad \text{---}(3.62)$$

$$\left(b_{\nu\nu} + \frac{1}{2}\frac{2\bar{b}}{a(\bar{\eta}_\nu)\cdot c(\bar{\eta}_\nu)\cdot T(\bar{\eta}_\nu)}\right)\bar{\gamma}_B(\bar{\eta}_\nu) = \frac{\alpha_B\left[T(\bar{\eta}_\nu)-1\right]}{2\,T(\bar{\eta}_\nu)} + \sum_{n=1}^{m}{}' b_{\nu n}\bar{\gamma}_B(\bar{\eta}_n) \quad \text{---}(3.63)$$

where the $\sum_{n=1}^{m}{}'$ denotes the summation for n going from 1 to m, but omitting the term $n = \nu$.

Values of $\bar{\eta}_\nu$ and the coefficients $b_{\nu\nu}$ and $b_{\nu n}$ are given by Multhopp[19], in which reference the following expressions are obtained.

$$b_{\nu\nu} = \frac{m+1}{4\sin\phi_\nu} \quad \text{------}(3.64)$$

$$b_{\nu n} = \begin{cases} \dfrac{\sin\phi_n}{(m+1)(\cos\phi_n - \cos\phi_\nu)^2} & \text{for } |n-\nu| = 1,3,5,\ldots \\ \text{or } = 0 & \text{for } |n-\nu| = 2,4,6,\ldots \end{cases} \quad \text{----}(3.65)$$

$$\bar{\eta}_n = \cos\phi_n = \cos\frac{n\pi}{m+1} \quad \text{------}(3.66)$$

Tables 1 and 2 give the values of η_n, $b_{\nu\nu}$, and $b_{\nu n}$ for $m = 7$ and 15. By solving the two systems of linear equations (3.62) and (3.63), values of $\bar{\gamma}_w$ and $\bar{\gamma}_B$ at spanwise positions $\bar{\eta}_n$ are obtained, and the sum of these two terms gives $\bar{\gamma}_{total}$.

From equation (3.9)

$$\gamma(\eta) = \frac{\bar{b}}{b} \cdot \bar{\gamma}(\bar{\eta}) \qquad (3.67)$$

and hence the non-dimensional circulation is known at the spanwise points η_n which are given by equations (3.59) and (3.66).

Finally, it is necessary to solve the equation (3.46).

$$\gamma(y) = \gamma(\bar{\eta}=0) + \frac{(\bar{z}_{us}-\bar{z}_{Ls})\left\{\bar{v}_{z i_T}(\bar{z}_w) + \frac{1}{2}\left(\frac{\partial \bar{v}_{z i}}{\partial \bar{z}}\right)_{\bar{z}=\bar{z}_w}\left(\bar{z}_{us}+\bar{z}_{Ls}-2\bar{z}_w\right)\right\}}{b V_0} \quad ---(3.46)$$

Consider the wing/body cross-section as shown in figure 6 and in particular the longitudinal section parallel to, and at a distance y from, the vertical plane of symmetry. From the conformal transformation,

$$\bar{z} = z\left[1 + \frac{R^2}{z^2+y^2}\right] \quad -------(3.68)$$

Over the body, which in this instance is taken as circular,

$$z^2+y^2 = R^2$$

$$\therefore \quad \bar{z} = 2z \quad -------(3.69)$$

Also, for a mid-wing configuration,

$$\bar{z}_w = 0 \quad ------(3.70)$$

From figure 6

$$z_{us} = -\sqrt{R^2-y^2} = -R\sqrt{1-\left(\frac{y}{R}\right)^2} \quad -------(3.71)$$

and also $\qquad z_{Ls} = -z_{us} \qquad$ -------(3.72)

$$\therefore z_{us}+z_{Ls} = 0 \quad \text{and} \quad z_{us}-z_{Ls} = -2R\sqrt{1-\left(\frac{y}{R}\right)^2} \quad -------(3.73)$$

$$\therefore \bar{z}_{us}-\bar{z}_{Ls} = -4R\sqrt{1-\left(\frac{y}{R}\right)^2} \quad -------(3.74)$$

Using equations (3.70), (3.73), and (3.74), equation (3.46) becomes:-

$$\gamma(y) = \gamma(\bar{\eta}=0) - \frac{2\bar{v}_{\gamma i_T}(\bar{\eta}=0)}{V_0} \cdot \frac{R}{b/2} \sqrt{1-\left(\frac{y}{R}\right)^2} \qquad \text{------}(3.75)$$

Thus the load over the body is the load at the wing/body junction reduced by the term $\frac{2\bar{v}_{\gamma i_T}}{V_0} \cdot \frac{R}{b/2} \sqrt{1-(y/R)^2}$.
Weber[16] suggests that this reduction should, in the case of a thick wing, be less than the value given here for the thin wing, and to allow for this she multiplies the above term by $\sqrt{k}$.

$$\gamma(y) = \gamma(\bar{\eta}=0) - \frac{2\bar{v}_{\gamma i_T}(\bar{\eta}=0)}{V_0} \cdot \frac{\sqrt{k}\, R}{b/2} \sqrt{1-\left(\frac{y}{R}\right)^2} \qquad \text{------}(3.76)$$

$$\text{Also, } \frac{\bar{v}_{\gamma i_T}(\bar{\eta}=0)}{V_0} = \bar{\alpha}_i = \frac{1}{\pi}\int_{-1}^{+1} \frac{d\bar{\gamma}}{d\bar{\eta}'} \cdot \frac{d\bar{\eta}'}{\bar{\eta}-\bar{\eta}'} \qquad \text{------}(3.77)$$

De Young[15] shows that, using the same quadrature formula as before, this integral becomes:-

$$\frac{\bar{v}_{\gamma i_T}(\bar{\eta}=0)}{V_0} = 2\left[b_{\nu\nu}\bar{\gamma}_\nu - \sum_{n=1}^{m}{}' b_{\nu n}\bar{\gamma}_n \right] \qquad \text{------}(3.78)$$

Physically, this is the downwash angle at an infinite distance downstream for any wing geometry.

It is of interest to consider a different approach to the problem of obtaining a numerical value for the integral in equation (3.77). By again splitting $\bar{\gamma}$ into two parts, $\bar{\gamma}_W$, and $\bar{\gamma}_B$, equation (3.77) can be written as

$$\frac{\bar{v}_{\gamma i_T}(\bar{\eta}=0)}{V_0} = \frac{1}{\pi}\int_{-1}^{+1} \frac{d\bar{\gamma}_W}{d\bar{\eta}'} \cdot \frac{d\bar{\eta}'}{\bar{\eta}-\bar{\eta}'} + \frac{1}{\pi}\int_{-1}^{+1} \frac{d\bar{\gamma}_B}{d\bar{\eta}'} \cdot \frac{d\bar{\eta}'}{\bar{\eta}-\bar{\eta}'} \qquad \text{---}(3.79)$$

From equations (3.33), (3.34), and (3.79), $\frac{\bar{v}_{\gamma_{i}T}(\bar{\eta}=0)}{V_0}$ can be expressed in terms of the circulation at the root, i.e. where $\bar{\eta}=0$:-

$$\frac{\bar{v}_{\gamma_i T}}{V_0} = \frac{1}{T(\bar{\eta}=0)}\left\{2\alpha_w + \alpha_B\left[T-1\right] - \frac{2\bar{b}}{a.c}\left(2\bar{\gamma}_w + \bar{\gamma}_B\right)\right\}_{root} \text{------}(3.80)$$

$$= \frac{1}{T(\bar{\eta}=0)}\left\{2\alpha_w + \alpha_B\left[T-1\right] - \frac{2b}{a.c}\left(2\gamma_w + \gamma_B\right)\right]_{root} \text{------}(3.81)$$

since, from equation (3.67),

$$\bar{b}\bar{\gamma} = b\gamma$$

Also, from equations (3.61) and (3.59),

$$T(\bar{\eta}=0) = 1+k \qquad \text{------}(3.82)$$

$$\therefore \frac{\bar{v}_{\gamma_i T}(\bar{\eta}=0)}{V_0} = \frac{1}{1+k}\left\{2\alpha_w + k\,\alpha_B - \frac{2b}{a.c}\left(2\gamma_w + \gamma_B\right)\right\}_{\bar{\eta}=0} \qquad \text{--}(3.83)$$

Equation (3.76) can now be solved at values of y between the centre-line and the wing/body junction, and hence a complete picture of the lift distribution over the semi-span is obtained.

The numerical solution of equations (3.62) and (3.63) is described in section 4.1.

4. NUMERICAL AND EXPERIMENTAL CONSIDERATIONS.

4.1 A DEUCE programme has been prepared to deal with equations (3.62) and (3.63). This programme is in three sections.

The first section, which is in α-code, evaluates the coefficients of $\bar{\gamma}_W(\bar{\eta}_\nu)$ and $\bar{\gamma}_B(\bar{\eta}_\nu)$ for a given set of parameter cards. As the coefficients of $\bar{\gamma}_W(\bar{\eta}_n)$ and $\bar{\gamma}_B(\bar{\eta}_n)$ are independent of the configuration under consideration, they are not calculated each time but comprise part of the ptogramme data pack. The first part of the output is made up of the coefficients for each term in the set of equations given by (3.62) and the second part consists of the corresponding coefficients for (3.63). If a wing alone case is being considered, there is no second part to the output.

The second section solves each set of simultaneous linear equatioms as given by the output from section 1, and the output gives the required values of $\bar{\gamma}(\bar{\eta}_\nu)$ in the binary system.

The last section converts thes binary values to decimal values which can then be tabulated.

Section 1 of the programme must be followed by one of three sets of data - the unchanging coefficients of $\bar{\gamma}_W(\bar{\eta}_n)$ and $\gamma_B(\bar{\eta}_n)$ -, the required set depending on whether a 7-point, 15-point, or 31-point solution is desired. After this set of data come the parameter cards specifying the nature of the wing/body configuration under consideration. Each set of parameter cards is of the form:-

1. (Body diam.) ÷ (Overall span) = $\frac{D}{b}$
2. Aspect Ratio = A
3. (Wing thickness) ÷ (Body radius) = $\frac{t}{R}$
4. $\frac{a_0}{\pi}$
5. Wing incidence = α_w°
6. Body incidence = α_B°
7. Angle of sweep of the quarter-chord line = $\phi_{c/4}^\circ$
8. $\frac{1+k'}{2}$
9. $1-k'$

where k' is the ratio $\frac{\text{tip chord}}{\text{centre chord}}$.

For the wing-alone case, parameter card 1. = $\frac{D}{b}$ is zero; and parameter card 3. = $\frac{t}{R}$ can have any value.

All three sections of the programme are continuous; i.e. they will each continue to run as long as parameter card sets - for section 1. - and coefficient card sets - for sections 2. and 3. - are fed in.

This procedure has been used to obtain the lift distributions shown in figures 7-10. The distribution has been given in the form $\left(\frac{C_L}{\alpha}\right)_{local}$ which is plotted against the non-dimensional spanwise unit η, and by measuring the area under such a curve, a value is obtained for the lift curve slope $\frac{dC_L}{d\alpha}$.

Calculations were carried out for a large selection of wings and wing/body combinations defined as follows:- Wings of aspect ratio = 2, 4, 6; sweep-back = 0°, 45°, 60°; and taper ratio = 1, 0.5, 0: without a body, and with bodies given by $\frac{D}{b}$ = 0.1, 0.2, 0.3. A thickness/chord ratio of 12% was used for all cases. $\frac{dC_L}{d\alpha}$ was then calculated for each case and the values are shown in tables 3, 4, and 5. For the cases with taper ratio = 1, these values were plotted against the aspect ratio for each angle of sweep as shown in figures 11-13. In order to indicate the actual effect which the body has on the total lift curve slope, the ratio $\left(\frac{C_{L\alpha}\text{ combination}}{C_{L\alpha}\text{ wing alone}}\right)$ has been plotted against the body size - given by $\frac{D}{b}$ - for each value of aspect ratio and sweep. These are shown in figures 14-16. Figures 17-28 are the corresponding graphs for taper ratio equal to 0.5 and 0.

4.2 A short series of wind tunnel tests was carried out to obtain some idea of the wing/body effect as it occurs in practice. Only total lift effects were considered, and from these the lift curve slope for each model was calculated.

The tests were made in a $3\frac{3}{4}$ ft. x $2\frac{3}{4}$ ft. wind tunnel and the wind speed was 85 ft./sec. which gave a Reynold's Number of 0.27×10^6 based on the wing chord.

The models were made of aluminium and consisted of three rectangular wings and two bodies, so designed that each wing could be tested with either body or without a body. The wings had 12 inch, 18 inch, and 24 inch spans and all had a chord of 6 inches giving aspect ratios of 2, 3, and 4 respectively. They were all of the same section - NACA 0012 - with straight tips. The bodies were solids of revolution with elliptic nose-sections and conical tail sections as shown in figure 33. One had a maximum diameter of 3 inches and a total length of $27\frac{1}{2}$ inches, and the other had a maximum diameter of $4\frac{1}{2}$ inches and a total length of $41\frac{1}{4}$ inches.

The models were mounted, as in figure 34, on a single mount at the wing quarter chord point on the fuselage axis, and were supported by a tail strut which was adjustable for incidence changes.

The total lift for each model was measured for a range of angles of incidence, in increments of one degree, and values of C_L were then calculated. These values appear in tables 6, 7, and 8, and, for the models of aspect ratio 3, they are also shown plotted against incidence in figure 35. It can be seen from this figure that the curves have the usual form as shown in the characteristic curves of Abbot & von Doenhoff[20] in which the slope noticeably increases at angles of incidence of two or three degrees on either side of the zero lift point. As this occurs both with the wing alone, and with the wing/body combinations, it cannot be due to the interference effects, and the lift curve slope given here refers to that at zero lift. Values of the lift curve slope for each model case could then be calculated, and these are shown in column 1 of table 9.

Before comparing these experimental values with those obtained theoretically, it is necessary to consider an additional lift which is experienced by the model but is not included in the theory. This lift increment is due to the finite length of the body and must, of course, always be present.

The tail section of the body is in the downwash field due to the trailing vortices from the wing and this must cause a decrease in the download which acts on this section of an isolated body. This download - or negative lift - is given by Multhopp[4] as :

$$L_T = -\frac{1}{2}\rho V_0^2 \alpha_{B_{eff}} \frac{\pi}{2} D^2$$

which gives a lift coefficient, referred to the wing area, of

$$C_{L_T} = -\alpha_{B_{eff}} \cdot \frac{\pi}{2} \frac{\left(\frac{D}{c}\right)^2}{A}$$

Now, the effective angle of incidence due to the trailing vortices can be written as α_i' and so the additional lift coefficient due to this effect is

$$\Delta C_L = \alpha_i' \cdot \frac{\pi}{2} \frac{\left(\frac{D}{c}\right)^2}{A}$$

At very low Reynold's Numbers, such as used in the present series of tests, it is reasonable to assume that there will be breakaway of the flow at the rear of the body resulting in a decrease of $\alpha_{B_{eff}}$ to zero. Since

$$\alpha_{B_{eff}} = \alpha_B - \alpha_i' \quad ,$$

α_i' must now become α_B and

$$\Delta C_L = \alpha_B \cdot \frac{\pi}{2} \frac{\left(\frac{D}{c}\right)^2}{A}$$

$$\therefore \Delta\left(\frac{dC_L}{d\alpha}\right) = \frac{\pi}{2} \frac{\left(\frac{D}{c}\right)^2}{A}$$

The experimental values of lift curve slope have thus been reduced by this term as shown in table 9, and in this table the calculated values are also shown.

5. ANALYSIS OF THEORETICAL AND EXPERIMENTAL RESULTS.

5.1 It is interesting to observe, from figures 14-16, that the introduction of a body does not necessarily result in a loss of lift, but rather that there is an optimum body diameter which can be as large as about 25% of the total wing span. This may seem somewhat unexpected because, in a wing/body combination, a part of the lift producing wing is replaced by a body which is not usually lift producing and hence a drop in total lift would be expected. However, when the body is at a positive angle of incidence, an upwash is produced around it; the wing is in this upwash field, and so experiences an additional lift mainly on that part of the wing close to the body since the upwash field weakens with distance from the body. This is shown in figure 8.
As already pointed out, over the actual body region there is a marked drop in lift, also shown in figure 8. In some cases, the lift increase due to the body upwash more than cancels this drop with the nett result of an increase in total lift.

Obviously, for a given chord, as the span increases - i.e. as the aspect ratio increases - the upwash field will produce an increasing addition to the lift produced by the wing itself. This can be seen from figures 14-16 where the body effect is more pronounced for the larger values of aspect ratio.

In the case of swept wings and wing/body combinations, an effect of the sweep is to cause the shedding of trailing vortices near the centre-line[21] or wing/body junction in the opposite sense to those shed nearer the tips, and this causes a decrease in the induced downwash at the centre-line or junction. The load reduction over the body is a function of this downwash and is thus also reduced causing an increase in total lift. Thus the body effect is more beneficial for swept wing/body combinations as can be seen by comparing corresponding curves from figures 14-16; this is also shown in figures 29 and 30.

A feature of tapered wings is that trailing vortices are shed as much near the centre section as near the tip, and this causes an increase in the induced downwash at the wing/body junction. Thus the load reduction over the body is increased and the total lift decreased. This can be seen by comparing corresponding curves from figures 14, 20, and 26 and it is also shown in figures 31 and 32. A mathematical form for this explanation of these effects of sweep-back and taper is given in chapter 6.

5.2 It can be seen from table 9 that the calculated values of the lift curve slope are considerably higher than the corresponding values obtained from the model tests. This is due to the fact that in the calculations the theoretical two-dimensional lift curve slope of 2π was used, while in practice the value is considerably lower than this. To overcome this difference, the ratio $\left(\frac{C_{L\alpha \text{ combination}}}{C_{L\alpha \text{ wing alone}}}\right)$ has been calculated for each case, and entered in table 9. This now shows that there is indeed a very good agreement between the experimental and the calculated values.

6. COMPARISONS AND CONCLUSIONS

6.1 The basic difference between the methods of Multhopp and Weber for unswept wing and wing/body combinations lies in the fact that Weber considers the induced downwash at the wing for that part of the wing covered by the fuselage to be twice the value used by Multhopp. Thus the values of $\gamma_W(\eta_\nu)$ are the same for both methods, but Weber gives a lower value of $\gamma_B(\eta_\nu)$. Over the outer region of the wing semi-span this difference is insignificant as the body effect is very small near the wing tips - except for wings of very small aspect ratio and large body size -, while over the inboard regions of the wing it will decrease the lift as shown in figure 7. For wing alone cases, these methods will be similar as shown in figure 8.

It is possible to justify this change made by Weber by considering a point on the wing, near the junction with the body. As can be seen from equation (2.24), Multhopp's theory is exactly equivalent to the wing alone case, except that the span of the wing becomes $\left[1-\left(\frac{D}{b}\right)^2\right]$ x the span of the combination, the chord becomes $R\left(\frac{d\bar{u}}{du}\right)$ x that of the combination, and the wing setting angle is altered by a factor $\frac{1}{R\left(\frac{d\bar{u}}{du}\right)}$. For the case of zero wing setting, these alterations can be illustrated as follows:-

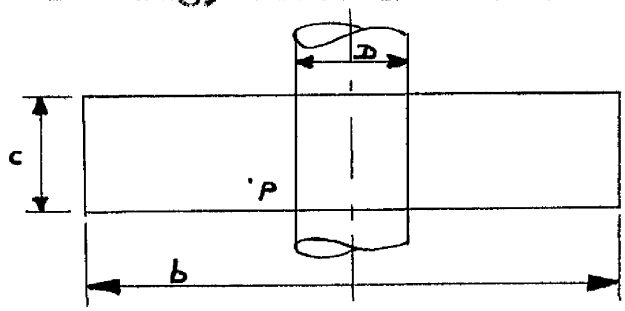

Wing/body combination

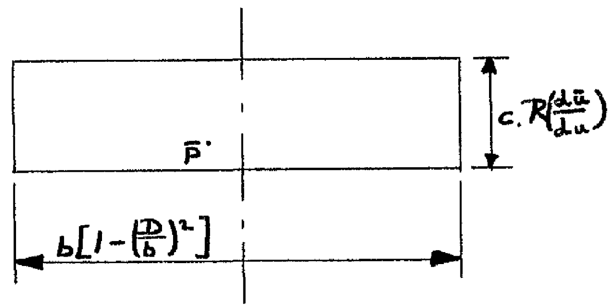

Equivalent wing alone

Consider a point P, near the wing/body junction, and its corresponding position, $\bar{P}$, on the equivalent wing alone. Let the induced downwash due to the trailing vortices be $\bar{v}_{\gamma_{i_T}}$ in the transformed Trefftz-plane. According to Multhopp, the induced downwash over the whole transformed wing is half this value. Thus he gives:

$$v_{\gamma_{i_P}} = \mathcal{R}\left(\frac{d\bar{u}}{du}\right) . \bar{v}_{\gamma_{i_{\bar{P}}}} = \frac{1}{2}\, \mathcal{R}\left(\frac{d\bar{u}}{du}\right) \bar{v}_{\gamma_{i_T}}$$

However, point P is within the region affected by the presence of the body and the upwash caused by it. Thus, in order to fulfil the boundary condition that there can be no velocity component normal to the surfaces of the wing and body, there must be an increase in the induced downwash to balance this increase in upwash due to the body, and so Weber gives:

$$v_{\gamma_{i_P}} = \mathcal{R}\left(\frac{d\bar{u}}{du}\right) . \bar{v}_{\gamma_{i_{\bar{P}}}} = \mathcal{R}\left(\frac{d\bar{u}}{du}\right) . \bar{v}_{\gamma_{i_T}}$$

This value is based on the fact that the body region can be considered as a wing of small aspect ratio, as explained in section 3.1 .

Hence equation (2.24) should now be replaced by equation (3.19), and it is obvious from this equation that there is no longer a simple wing alone which can be taken as equivalent to the wing/body combination.

As already pointed out, Multhopp overestimates the lift on the inboard region of the wing when he uses the equivalent wing alone method, and so it is to be expected that Luckert, whose method uses an analogy depending on the conception of an equivalent wing alone, should also overestimate the lift in these regions as shown in figure 7.

It was shown in section 3.6 that the load over the body is the load at the wing/body junction reduced by a term which is a function of $\frac{\bar{v}_{\gamma i T}}{V_0}$. From equation (3.83) it can be seen that, if the value of $\gamma(\bar{\eta}=0)$ is overestimated, the value of $\frac{\bar{v}_{\gamma i T}}{V_0}$ is underestimated, and so the load reduction obtained at the centre-line will be less than it should be. This is shown in figure 7, where the value obtained by Luckert for $\left(\frac{C_L}{\alpha}\right)_{local}$ at the centre-line is considerably higher than that obtained by the method discussed in this paper. Thus the values obtained by Luckert for $\frac{dC_L}{d\alpha}$ for a wing/body combination - given by the area under curves of the form of figure 7 - are higher than they should be, as is shown in figure 14.

Also contributing to this difference is the fact that Luckert obtains values of the lift curve slope for the wing alone which are considerably lower than those obtained in this paper. In the absence of a body, Luckert's method corresponds exactly to that of De Young whose lift distribution is shown in figure 9 for a wing of aspect ratio 3 and sweep-back 45°. Also shown in the figure are the values obtained from the present method and some experimental points obtained from references 22 and 23. The corresponding values of the lift curve slope are given below:

Aspect ratio = 3, $\phi_{c/4} = 45°$, no taper	
Present method	2.93
De Young's method	2.56
Reference 22	2.90
Reference 23	2.81

Figure 10 also shows that the prediction of the present method is more realistic than that of De Young for aspect ratios of 2 and 5, although at the lower aspect ratio, the measured values of lift are lower than those predicted, suggesting that the assumption of constant induced downwash over the chord, as made in chapter 3, is not valid for aspect ratios as low as 2.

6.2 As has already been pointed out, the reduction of the lift over the diameter of the body is dependent upon the value of $\frac{\bar{v}_{\gamma i \tau}}{V_0}$ at the root, and an expression is given for this term by equation (3.83) :

$$\frac{\bar{v}_{\gamma i}}{V_0}\tau(\bar{\eta}=0) = \frac{1}{1+k}\left\{\lambda\alpha_w + k\alpha_B - \frac{2b}{a.c}\left(2\gamma_w + \gamma_B\right)\right\}_{\bar{\eta}=0} \qquad \text{--(3.83)}$$

At the root position, the value to be used in this equation for $a(\bar{\eta}=0)$ is dependent upon the angle of sweep as is given in equation (3.23) :

$$a_c = a_0\left(1 - \frac{\phi_{c/2}}{\pi/2}\right)$$

Thus, as the angle of sweep increases, the required value of a is decreased, with the result that the lift reduction over the body is also decreased, as stated in chapter 5.

For a given aspect ratio and angle of sweep, an increase in taper results in an increase in the root chord and so, from equation (3.83), the lift reduction over the body will be increased resulting in a lower value of total lift, again as given in the previous chapter.

In order to understand more fully these effects of sweep and taper, it is helpful to consider the vortex system corresponding to each planform. As a transformation is first carried out, in the present theory, to replace the body with a vertical slit, the following explanation will assume that there is no body present.

For the rectangular wing there is very little shedding of trailing vortices near the centre section, and the sense of those which are shed is shown in figure 36. Near the centre section of swept wings, the vorticity vector curves from the spanwise direction to cut the centre-line at right angles[21]. This causes some vortices to be shed near the centre, and, as seen in figure 37, these are of the opposite sense to those shed near the tips. For the unswept, tapered wing, the vortices are shed over the whole semi-span and they all have the same sense as shown in figure 38.

Thus at the centre-line of swept wings the induced downwash is decreased by these inboard vortices, while for tapered wings it is increased by them.

6.3 An attempt has been made in this paper to examine a number of methods for calculating lift and lift distributions for wing/body combinations. The method suggested by Multhopp, with the extensions proposed by Weber, Kirby, and Kettle, appears to give the most satisfactory results. It is particularly useful because it is applicable to thin or thick wings with sweep and taper as well as to straight rectangular wings, and it can also be used for cases with a wing setting angle.

Calculations using this method have been carried out for a wide variety of wing/body combinations and the results are given in graphical form. It was found from these graphs that the body effect could sometimes increase the total lift -- this being more pronounced for higher values of sweep, and less pronounced for increasingly tapered wings.

Luckert, whose method in its present form is only applicable to unswept wings, overestimates this body effect, while the methods of Lennertz and Spreiter are both only valid for a very small range of wing planform.

REFERENCES

1. B.M.Jones	The importance of "streamlining" in relation to performance. R.& M. 1115 1923.
2. J.Lennertz	Influence of the airplane body on the wings. Aerodynamic Theory, Vol.IV, Div.K, Chap.3; edited by W.F.Durand 1943.
3. P.A.Pepper	Minimum induced drag in wing-fuselage interference. NACA TN 812 1941.
4. H.Multhopp	Aerodynamics of the fuselage. R.T.P. Trans. No. 1220 1941.
5. M.Zlotnick and S.W.Robinson	A simplified mathematical model for calculating aerodynamic loading and downwash for midwing wing-fuselage combinations with wings of arbitrary planform. NACA RM L52J27a 1953.
6. J.R.Spreiter	Aerodynamic properties of slender wing-body combinations at subsonic, transonic, and supersonic speeds. NACA TN 1662 1948.
7. R.T.Jones	Properties of low-aspect-ratio pointed wings at speeds below and above the speed of sound. NACA Report No. 835 1946.
8. H.R.Lawrence	The aerodynamic characteristics of low-aspect-ratio wing-body combinations in steady subsonic flow. Cornell Aero. Lab. Report No. AF-743-A-6 1952.
9. H.R.Lawrence and A.H.Flax	Wing-body interference at subsonic and supersonic speeds - survey and new developments. Journal of the Aeronautical Sciences, Vol.21 No. 5, pp.289-323 1954.

10. M.M.Munk	The aerodynamic forces on airship hulls. NACA Report No.184 1924.
11. H.Glauert	The elements of aerofoil and airscrew theory. Cambridge University Press 1943.
12. H.Lamb	Hydrodynamics. Cambridge University Press 1945.
13. H.J.Luckert	Lift and lift distribution of wings in combination with slender bodies of revolution. Annual General Meeting of the C.A.I., Toronto 1955.
14. J.Weissinger	The lift distribution of swept-back wings. NACA TM 1120 1947.
15. J.De Young and C.W.Harper	Theoretical symmetric span loading at subsonic speeds for wings having arbitrary plan form. NACA Report No.921 1948.
16. J.Weber, D.A.Kirby, and D.J.Kettle	An extensionsof Multhopp's method of calculating the spanwise loading of wing-fuselage combinations. R.& M. 2872 1951.
17. B.Thwaites	Incompressible Aerodynamics, chapter VIII. Oxford University Press 1960.
18. D.Küchemann	A simple method for calculating the span and chordwise loadings on thin swept wings. R.A.E. Report Aero 2392 1950.
19. H.Multhopp	The calculation of the lift distribution of aerofoils. R.T.P. Trans. No.2392 1938.
20. I.H.Abbott and A.E.von Doenhoff	Theory of wing sections. McGraw Hill 1949.

21. D. Küchemann — A simple method for calculating the span and chordwise loading on straight and swept wings of any given aspect ratio at subsonic speeds. R.& M. 2935 1952.

22. D. Küchemann, J. Weber, and G.G. Brebner — Low speed tests on 45-deg. swept-back wings. R.& M. 2882 1951.

23. V.M. Falkner, and D.E. Lehrian — Low speed measurements of the pressure distribution at the surface of a swept-back wing. R.& M. 2741 1949.

APPENDIX 1.

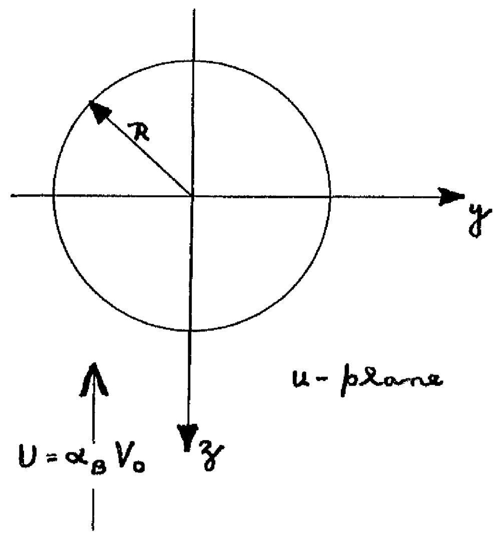

From the consideration of the flow of velocity $\alpha_B V_o$ past a circular cylinder of radius R, it is known that the complex potential, w, is given by

$$w = \alpha_B V_o \left(u + \frac{R^2}{u} \right) \qquad \text{------(A.1)}$$

$$= \alpha_B V_o \, \bar{u} \qquad \text{------(A.2)}$$

since the transformation from the u-plane to the $\bar{u}$-plane is $\bar{u} = u + \frac{R^2}{u}$.

$$\therefore \quad \frac{dw}{d\bar{u}} = \alpha_B V_o \qquad \text{------(A.3)}$$

Now, $\frac{dw}{du} = \frac{dw}{d\bar{u}} \cdot \frac{d\bar{u}}{du} = \alpha_B V_o \frac{d\bar{u}}{du}$ ------(A.4)

In the u-plane

$$\frac{dw}{du} = \frac{\partial \phi}{\partial z} + i \frac{\partial \psi}{\partial z} \qquad \text{------(A.5)}$$

$$\therefore \quad \frac{\partial \phi}{\partial z} = \mathcal{R}\left(\frac{dw}{du}\right) \qquad \text{------(A.6)}$$

$$= \alpha_B V_o \, \mathcal{R}\left(\frac{d\bar{u}}{du}\right) \qquad \text{------(A.7)}$$

Also,

$$v_z = - \frac{\partial \phi}{\partial z} \qquad \text{------(A.8)}$$

$$= - \alpha_B V_o \, \mathcal{R}\left(\frac{d\bar{u}}{du}\right) \qquad \text{------(A.9)}$$

If the body is now considered to be vanishingly small, $\mathcal{R}\left(\frac{d\bar{u}}{du}\right)$ becomes unity, and

$$v_z = -\alpha_B V_0 \qquad \text{--------(A.10)}$$

Therefore the effect of the body, or the downwash v_{z_B} due to it, is given by the difference between expressions (A.9) and (A.10) :-

$$v_{z_B} = -\alpha_B V_0 \left[\mathcal{R}\frac{d\bar{u}}{du} - 1\right] \qquad \text{--------(A.11)}$$

where the negative sign indicates that it is actually an upwash.

TABLE 1

ν	1	3	5	7
η_ν	0.9239	0.3827	-0.3827	-0.9239
$b_{\nu\nu}$	5.2262	2.1648	2.1648	5.2262
$b_{\nu n}$				
$n=2$	1.8810	0.8398	0.0744	0.0332
4	0.1464	0.8536	0.8536	0.1464
6	0.0332	0.0744	0.8598	1.8810
ν	2	4	6	
η_ν	0.7071	0.0000	-0.7071	
$b_{\nu\nu}$	2.8284	2.0000	2.8284	
$b_{\nu n}$				
$n=1$	1.0180	0.0560	0.0180	
3	1.0972	0.7887	0.0973	
5	0.0973	0.7887	1.0972	
7	0.0180	0.0560	1.0180	

TABLE 2

ν	1	3	5	7	
η_ν	0.9808	0.8315	0.5556	0.1951	$-\eta_\nu$
$b_{\nu\nu}$	20.5030	7.1998	4.8107	4.0786	$b_{\nu\nu}$
$b_{\nu n}$					
$n=2$	7.3858	2.8008	0.1763	0.0450	=14
4	0.5900	2.8575	1.9246	0.1686	12
6	0.1614	0.2867	1.9319	1.6409	10
8	0.0650	0.0904	0.2025	1.6422	8
10	0.0311	0.0392	0.0656	0.1730	6
12	0.0155	0.0187	0.0277	0.0543	4
14	0.0066	0.0078	0.0109	0.0191	$n=$ 2
	15	13	11	9	ν
ν	2	4	6	8	
η_ν	0.9239	0.7071	0.3827	0.0000	$-\eta_\nu$
$b_{\nu\nu}$	10.4525	5.6568	4.3295	4.0000	$b_{\nu\nu}$
$b_{\nu n}$					
$n=1$	3.7653	0.1628	0.0341	0.0127	=15
3	4.0661	2.2451	0.1724	0.0502	13
5	0.3831	2.2632	1.7386	0.1684	11
7	0.1154	0.2538	1.7418	1.6105	9
9	0.0490	0.0753	0.1836	1.6105	7
11	0.0238	0.0326	0.0590	0.1684	5
13	0.0113	0.0147	0.0236	0.0502	3
15	0.0034	0.0043	0.0066	0.0127	$n=$ 1
	14	12	10	8	ν

$A/\phi^\circ_{c/4}$	$\frac{D}{b} = 0$		0.1		0.2		0.3	
	I	II	I	II	I	II	I	II
2/0	3.03	1.0	3.02	0.997	2.96	0.977	2.72	0.897
4/0	4.04	1.0	4.14	1.028	4.14	1.028	3.86	0.956
6/0	4.56	1.0	4.78	1.049	4.82	1.058	4.47	0.981
2/45	2.49	1.0	2.53	1.016	2.55	1.024	2.42	0.972
4/45	3.14	1.0	3.28	1.045	3.34	1.063	3.28	1.045
6/45	3.43	1.0	3.64	1.061	3.80	1.108	3.77	1.099
2/60	2.08	1.0	2.13	1.024	2.17	1.042	2.12	1.019
4/60	2.47	1.0	2.61	1.056	2.69	1.089	2.69	1.089
6/60	2.61	1.0	2.84	1.088	2.96	1.133	2.96	1.133

Table 3. untapered; thickness/chord = 12% ; $a_0 = 2\pi$

$A/\phi^\circ_{c/4}$	$\frac{D}{b} = 0$		0.1		0.2		0.3	
	I	II	I	II	I	II	I	II
2/0	3.12	1.0	3.10	0.994	2.94	0.942	2.61	0.837
4/0	4.17	1.0	4.21	1.010	4.04	0.969	3.59	0.861
6/0	4.66	1.0	4.81	1.032	4.65	0.998	4.13	0.886
2/45	2.63	1.0	2.64	1.004	2.54	0.966	2.29	0.871
4/45	3.22	1.0	3.31	1.028	3.26	1.012	2.99	0.929
6/45	3.48	1.0	3.66	1.052	3.62	1.040	3.38	0.971
2/60	2.24	1.0	2.26	1.009	2.18	0.973	1.97	0.879
4/60	2.50	1.0	2.60	1.040	2.58	1.032	2.42	0.968
6/60	2.62	1.0	2.78	1.061	2.80	1.069	2.67	1.019

Table 4. taper = 0.5; thickness/chord = 12%; $a_0 = 2\pi$

$A/\phi^\circ_{c/4}$	$\frac{D}{b} = 0$		0.1		0.2		0.3	
	I	II	I	II	I	II	I	II
2/0	2.98	1.0			2.70	0.906	2.29	0.769
4/0	3.98	1.0	3.89	0.977	3.58	0.899	2.94	0.739
6/0	4.44	1.0	4.51	1.016	4.13	0.930	3.33	0.750
2/45	2.55	1.0			2.30	0.902	1.93	0.755
4/45	3.05	1.0	3.03	0.993	2.81	0.921	2.34	0.767
6/45	3.34	1.0	3.42	1.024	3.18	0.952	2.63	0.787
2/60	2.15	1.0			1.93	0.898	1.60	0.744
4/60	2.30	1.0	2.31	1.004	2.16	0.939	1.81	0.787
6/60	2.46	1.0	2.54	1.033	2.40	0.976	2.01	0.818

Table 5. taper = 0; thickness/chord = 12%; $a_0 = 2\pi$

$$\mathrm{I} \equiv \frac{dC_L}{d\alpha} \;; \qquad \mathrm{II} \equiv \left[\frac{dC_L}{d\alpha}(\text{combination})\right] \div \left[\frac{dC_L}{d\alpha}(\text{wing alone})\right]$$

Values of C_L

Aspect ratio = 2

Incidence°	Wing/alone	Wing+3"Body	Wing+4½"Body
-10	-0.515	-0.564	-0.572
- 9	-0.487	-0.531	-0.524
- 8	-0.441	-0.478	-0.475
- 7	-0.394	-0.444	-0.429
- 6	-0.351	-0.396	-0.381
- 5	-0.306	-0.347	-0.336
- 4	-0.253	-0.293	-0.281
- 3	-0.188	-0.237	-0.229
- 2	-0.154	-0.182	-0.179
- 1	-0.104	-0.141	-0.128
0	-0.061	-0.079	-0.080
1	-0.013	-0.024	-0.030
2	+0.031	+0.021	+0.010
3	0.074	0.065	0.051
4	0.117	0.111	0.097
5	0.165	0.162	0.146
6	0.218	0.218	0.203
7	0.265	0.273	0.252
8	0.310	0.325	0.297
9	0.353	0.379	0.343
10	0.391	0.412	0.386
11	0.435	0.454	0.434
12	0.468	0.493	0.470
13	0.494	0.530	0.510
14	0.518	0.561	0.554
15	0.544	0.592	0.594

TABLE 6

Values of C_L

Aspect ratio = 3

Incidence°	Wing/alone	Wing+3"Body	Wing+$4\frac{1}{2}$"Body
-10	-0.675	-0.673	-0.652
- 9	-0.630	-0.629	-0.641
- 8	-0.585	-0.598	-0.605
- 7	-0.532	-0.549	-0.560
- 6	-0.479	-0.498	-0.510
- 5	-0.421	-0.442	-0.456
- 4	-0.355	-0.371	-0.392
- 3	-0.287	-0.302	-0.322
- 2	-0.219	-0.226	-0.245
- 1	-0.153	-0.153	-0.175
0	-0.092	-0.082	-0.110
+ 1	-0.036	-0.024	-0.051
2	+0.020	+0.036	+0.004
3	0.077	0.093	0.067
4	0.125	0.150	0.127
5	0.183	0.220	0.198
6	0.248	0.296	0.275
7	0.317	0.371	0.346
8	0.376	0.428	0.405
9	0.428	0.480	0.458
10	0.478	0.530	0.512
11	0.522	0.578	0.562
12	0.567	0.621	0.607
13	0.604	0.654	0.650
14	0.637	0.677	0.657
15	0.663	0.693	0.661

TABLE 7

Values of C_L

Aspect ratio = 4

Incidence°	Wing/alone	Wing+3"Body	Wing+4½"Body
-10	-0.767	-0.730	-0.663
- 9	-0.728	-0.713	-0.646
- 8	-0.678	-0.689	-0.591
- 7	-0.625	-0.652	-0.531
- 6	-0.566	-0.595	-0.463
- 5	-0.511	-0.536	-0.385
- 4	-0.436	-0.471	-0.291
- 3	-0.360	-0.394	-0.200
- 2	-0.281	-0.306	-0.118
- 1	-0.194	-0.219	-0.050
0	-0.135	-0.143	+0.014
1	-0.070	-0.071	0.085
2	-0.011	-0.004	0.158
3	+0.051	+0.062	0.241
4	0.108	0.128	0.325
5	0.181	0.208	0.406
6	0.263	0.299	0.477
7	0.350	0.388	0.542
8	0.416	0.457	0.602
9	0.477	0.520	0.658
10	0.528	0.576	0.706
11	0.577	0.626	0.750
12	0.624	0.663	0.736
13	0.663	0.682	0.710
14	0.696	0.697	
15	0.728	0.705	

TABLE 8

	$\frac{dC_L}{d\alpha}$ (exp)	Tail effect	Amended $\frac{dC_L}{d\alpha}$ (exp.)	$\frac{dC_L}{d\alpha}$ (calc)	$\frac{C_{L\alpha}\text{ (combination)}}{C_{L\alpha}\text{ (wing alone)}}$ exp.	calc.
Aspect ratio = 2						
Wing alone	2.52	0	2.52	3.03	1.0	1.0
Wing+3"body	2.58	0.20	2.38	2.86	0.94	0.94
Wing+4½"body	2.32	0.35	1.97	2.35	0.78	0.78
Aspect ratio = 3						
Wing alone	3.21	0	3.21	3.63	1.0	1.0
Wing+3"body	3.38	0.13	3.25	3.68	1.01	1.01
Wing+4½"body	3.38	0.23	3.15	3.52	0.98	0.97
Aspect ratio = 4						
Wing alone	3.50	0	3.50	4.04	1.0	1.0
Wing+3"body	3.82	0.10	3.72	4.19	1.06	1.04
Wing+4½"body	3.87	0.18	3.69	4.15	1.05	1.03

TABLE 9

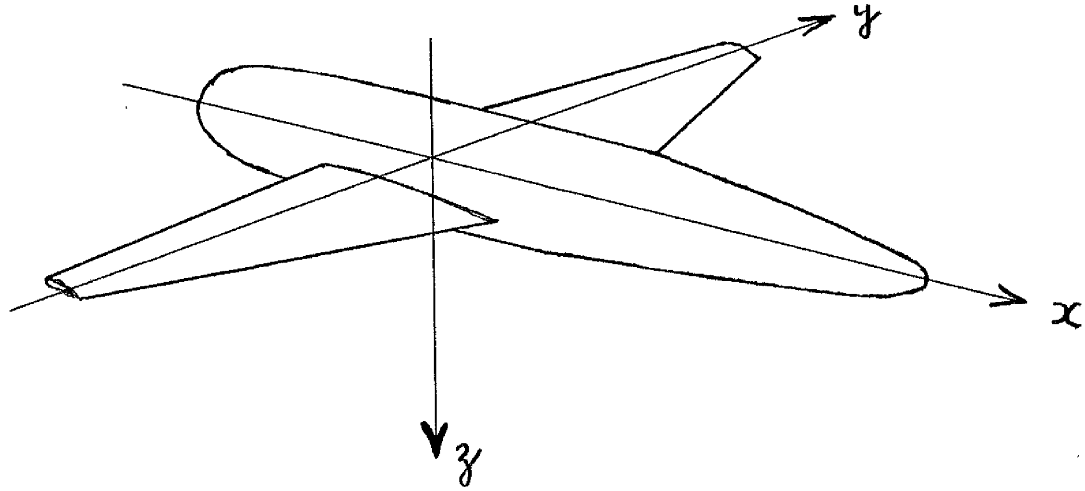

Fig. 1

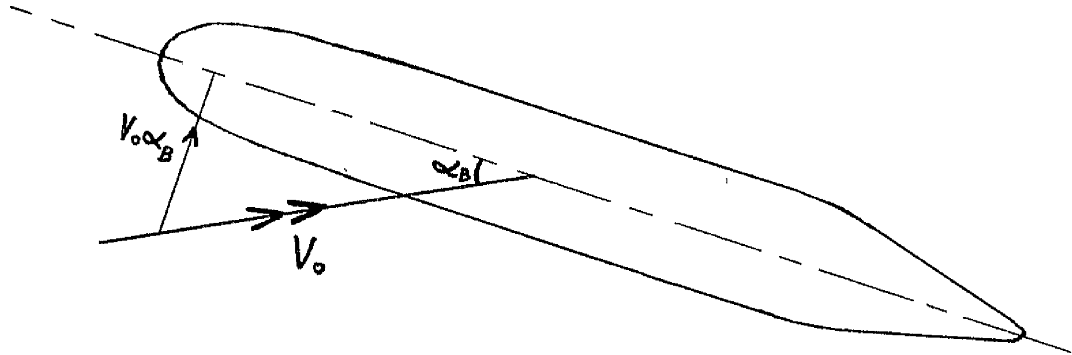

Fig. 2

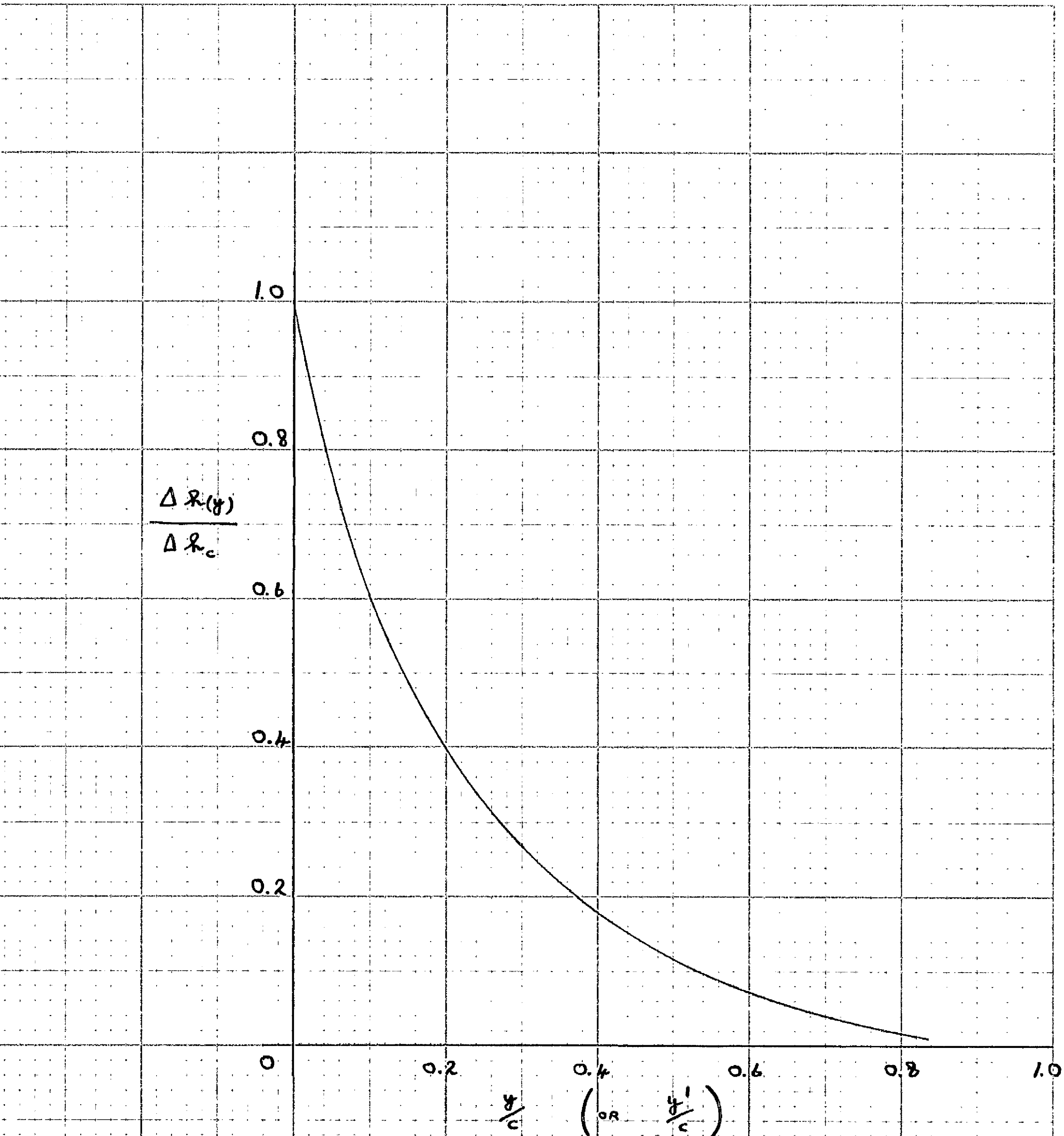

Fig. 3

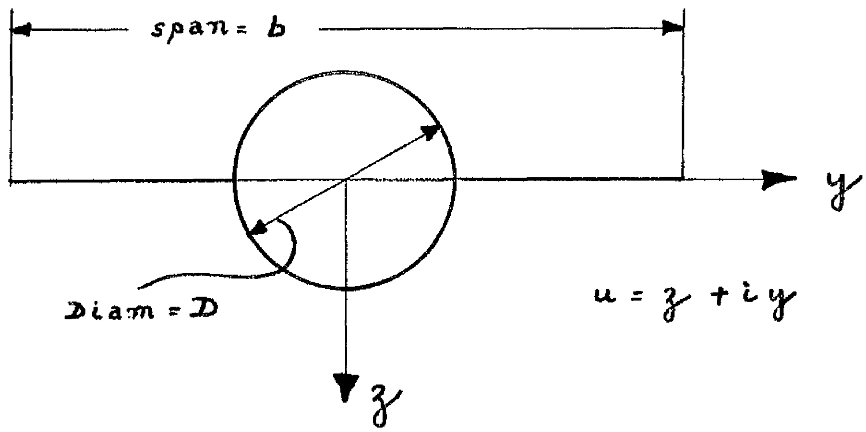

Fig. 4

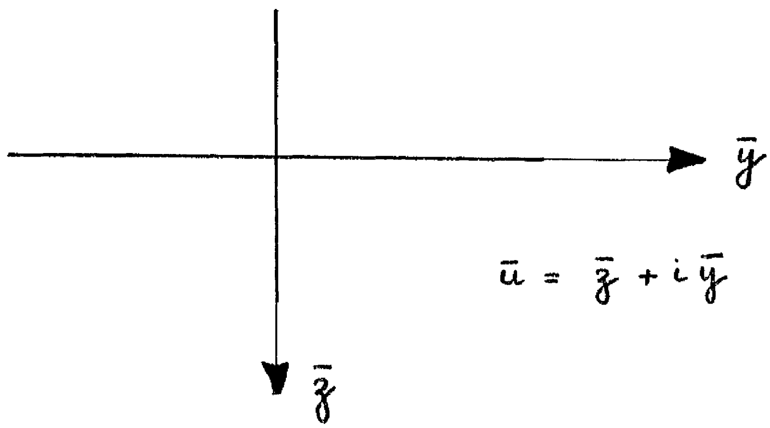

Fig. 5

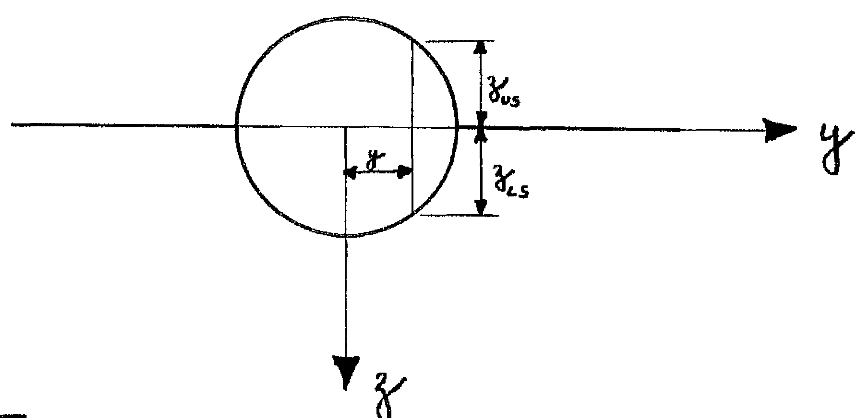

Fig. 6

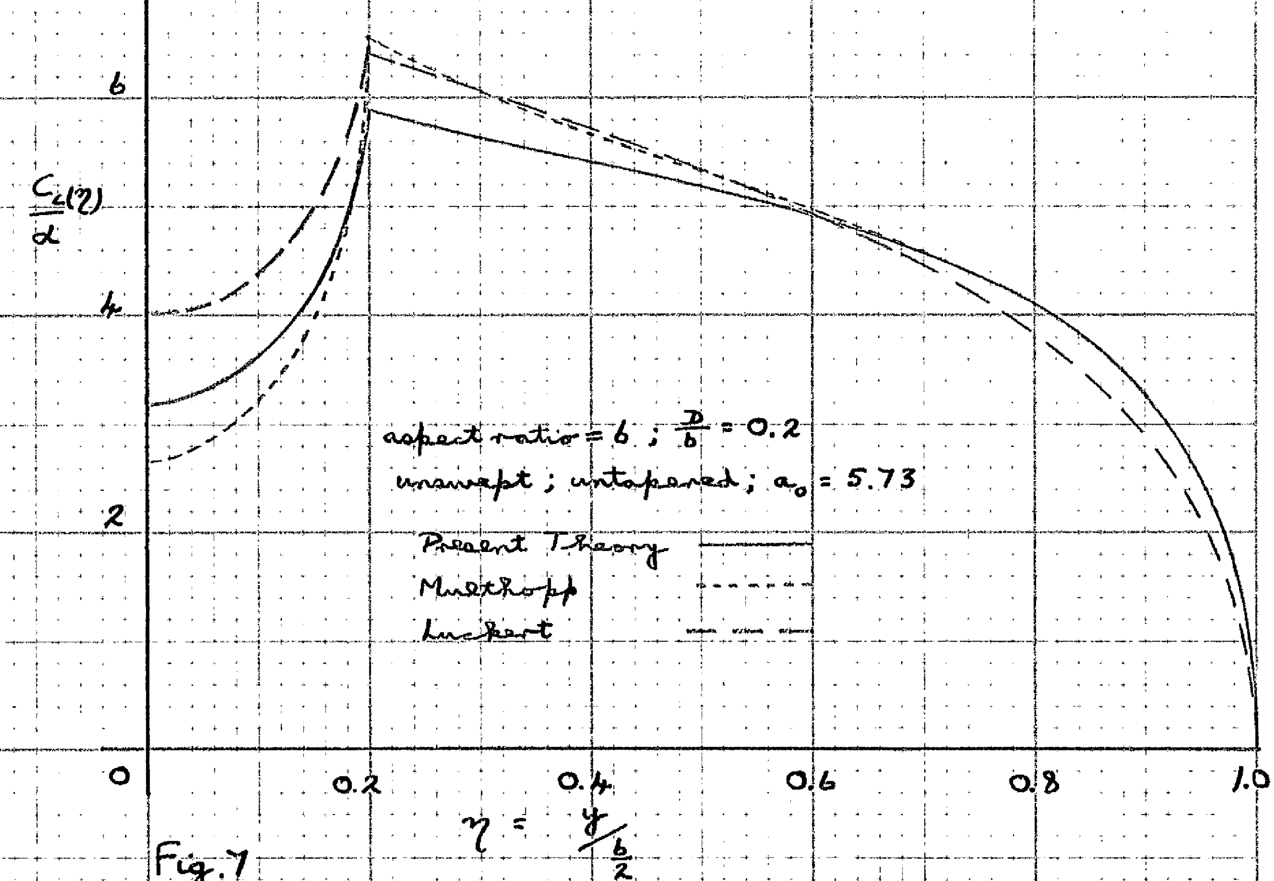

6
4
2
0
$\frac{C_L(\eta)}{\alpha}$
aspect ratio = 6 ; $\frac{D}{b}$ = 0.2
unswept ; untapered ; a_0 = 5.73
Present Theory
Multhopp
Lucket
0.2
0.4
0.6
0.8
1.0
$\eta = \frac{y}{b/2}$

Fig. 7

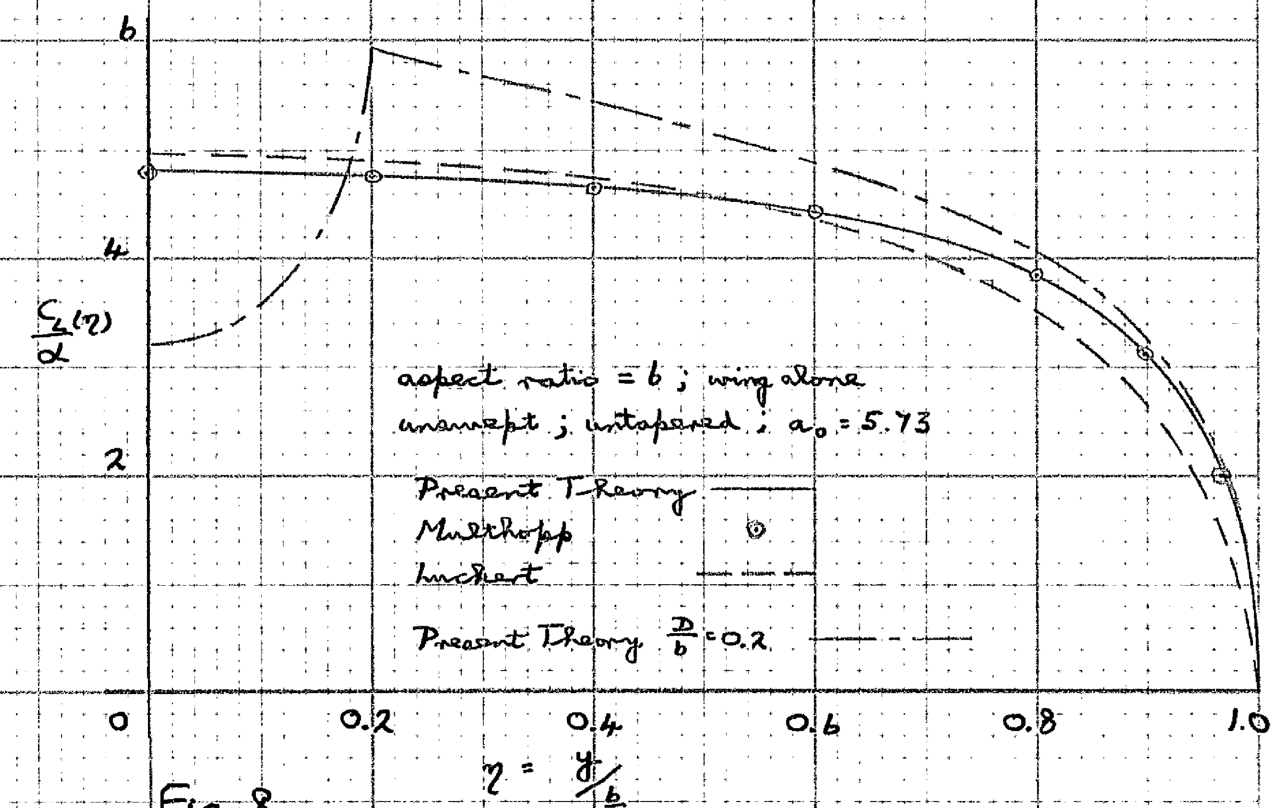

6
4
2
0
$\frac{C_L(\eta)}{\alpha}$
aspect ratio = 6 ; wing alone
unswept ; untapered ; a_0 = 5.73
Present Theory
Multhopp
Lucket
Present Theory $\frac{D}{b}$ = 0.2
0.2
0.4
0.6
0.8
1.0
$\eta = \frac{y}{b/2}$

Fig. 8

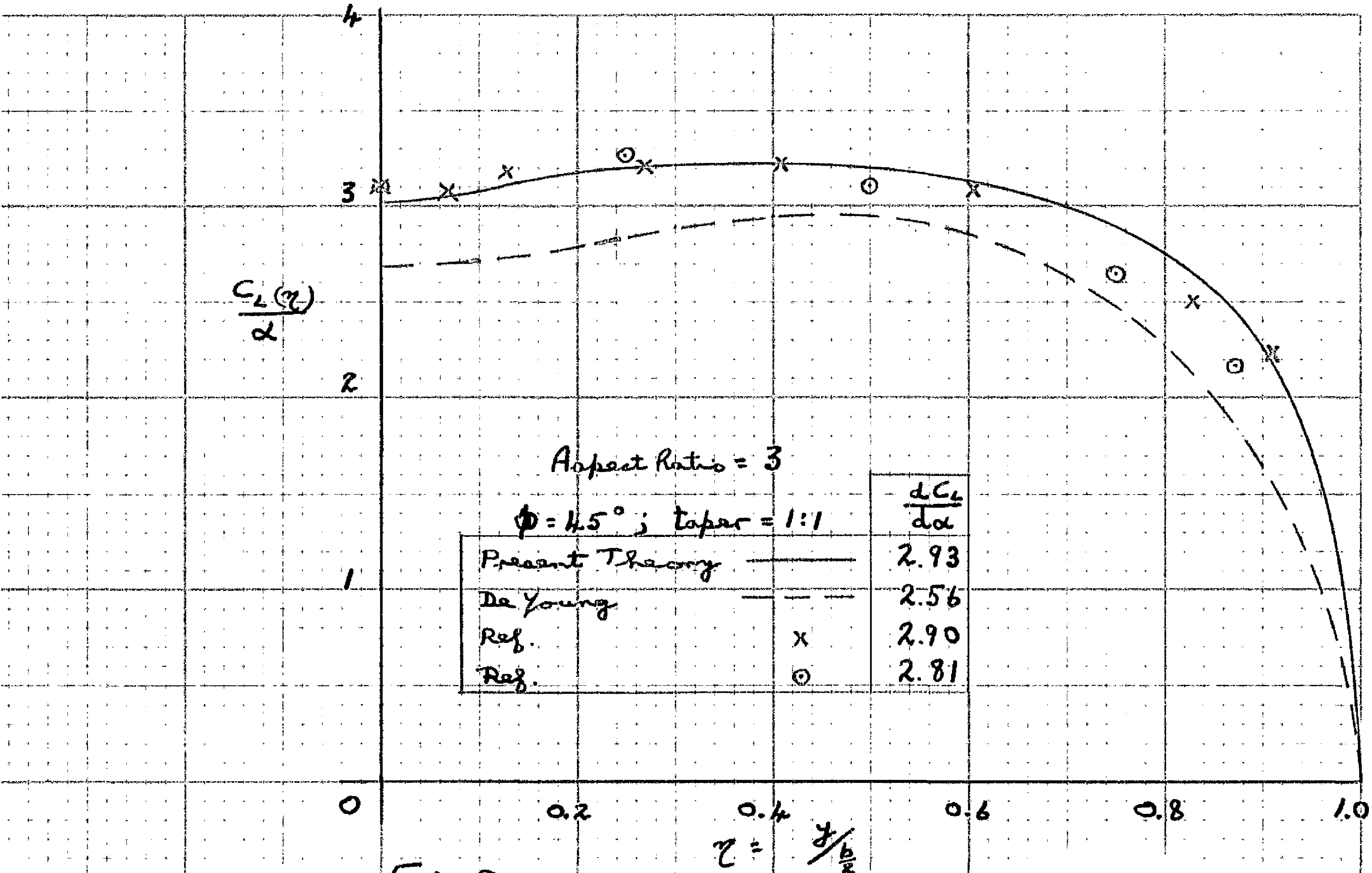
4
3
2
1
0
$\frac{C_L(\eta)}{\alpha}$
Aspect Ratio = 3
$\phi = 45°$; taper = 1:1
$\frac{dC_L}{d\alpha}$
Present Theory 2.93
De Young 2.56
Ref. x 2.90
Ref. ⊙ 2.81
0.2
0.4
0.6
0.8
1.0
$\eta = y/\frac{b}{2}$

Fig. 9

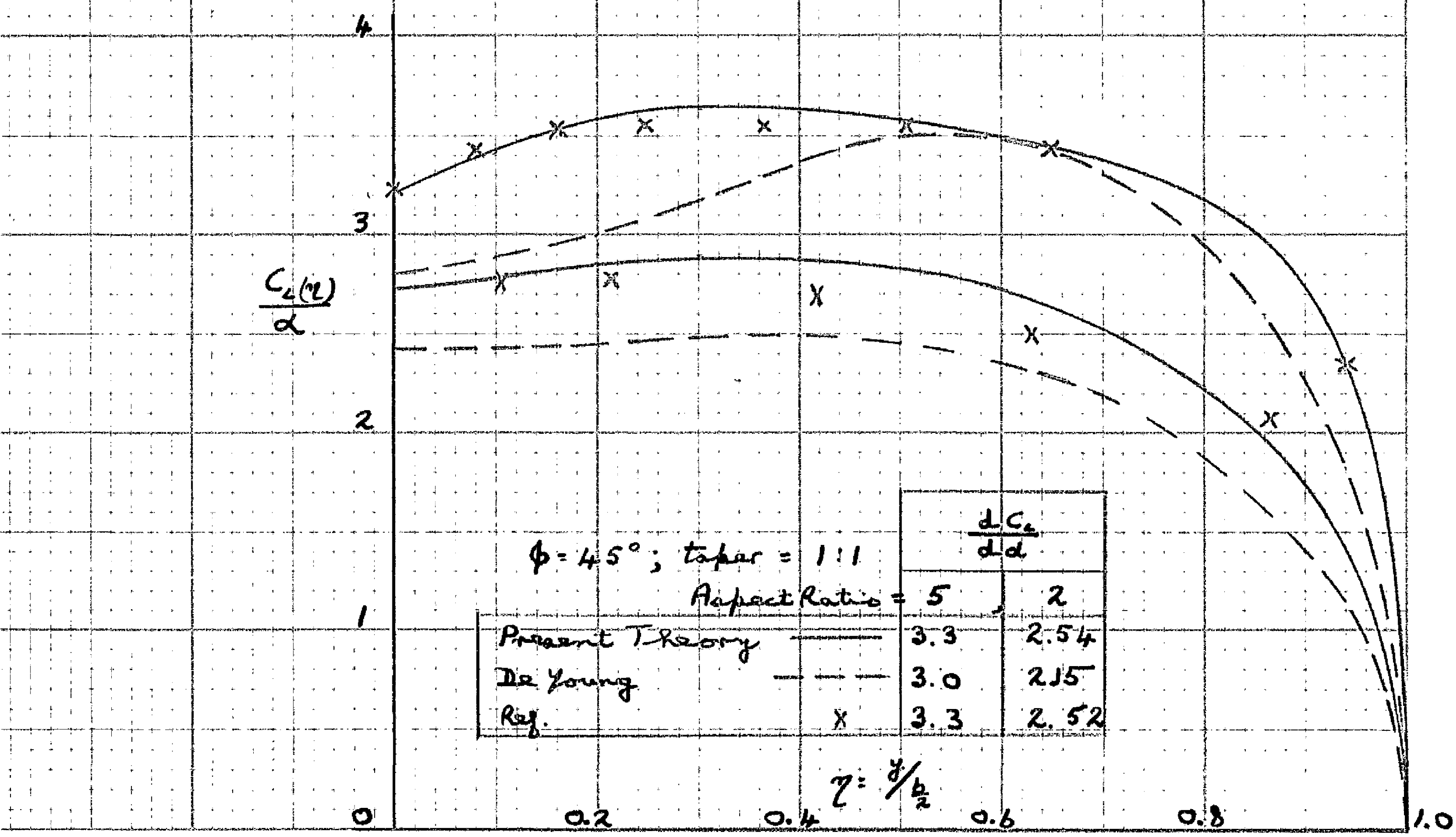
4
3
2
1
0
$\frac{C_L(\eta)}{\alpha}$
$\phi = 45°$; taper = 1:1
$\frac{dC_L}{d\alpha}$
Aspect Ratio = 5, 2
Present Theory 3.3 2.54
De Young 3.0 2.15
Ref. x 3.3 2.52
$\eta = y/\frac{b}{2}$
0.2
0.4
0.6
0.8
1.0

Fig. 10

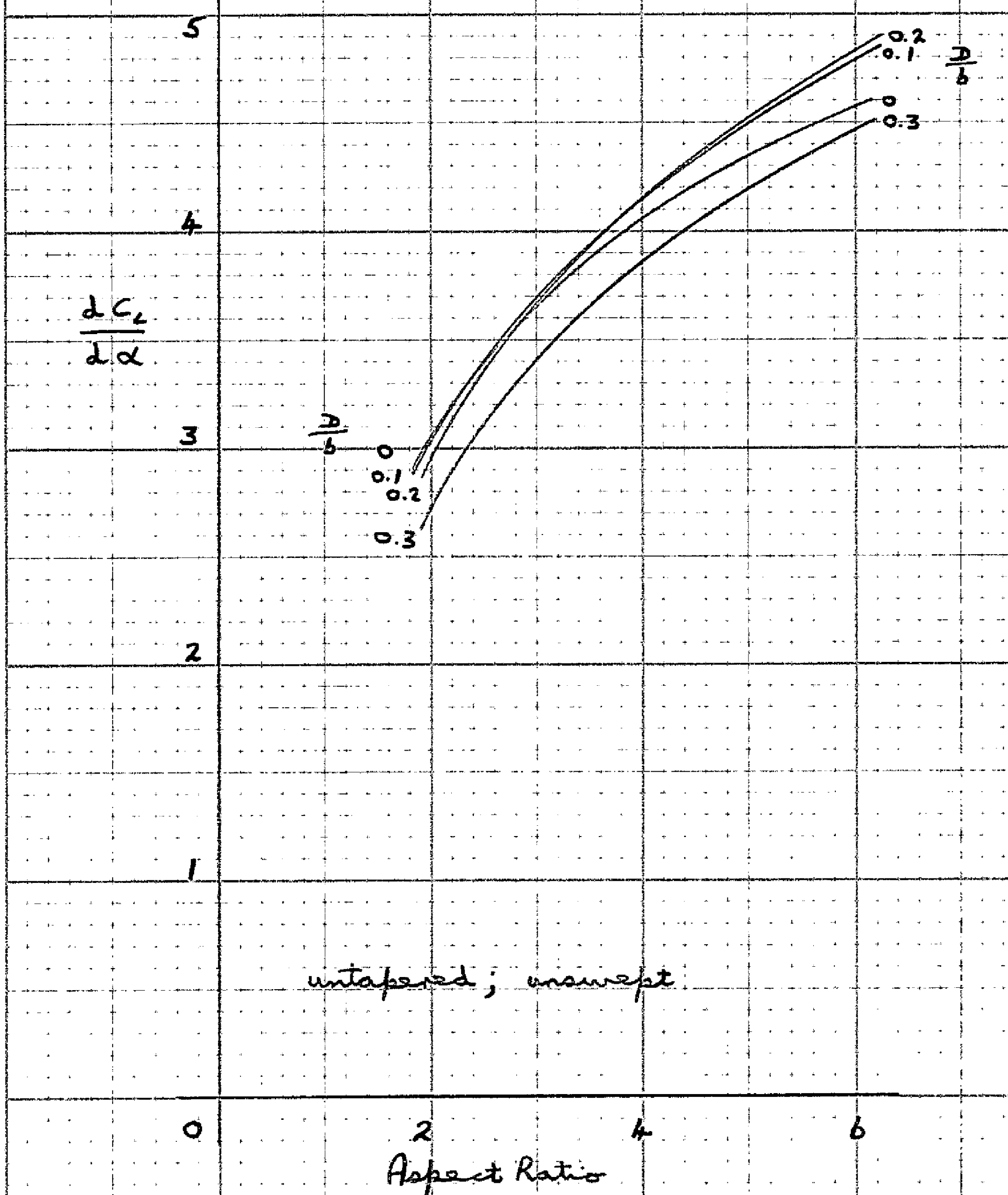

$\frac{dC_L}{d\alpha}$
5
4
3
2
1
0
2
4
6
Aspect Ratio
$\frac{D}{b}$
0
0.1
0.2
0.3
untapered; unswept

Fig. 11

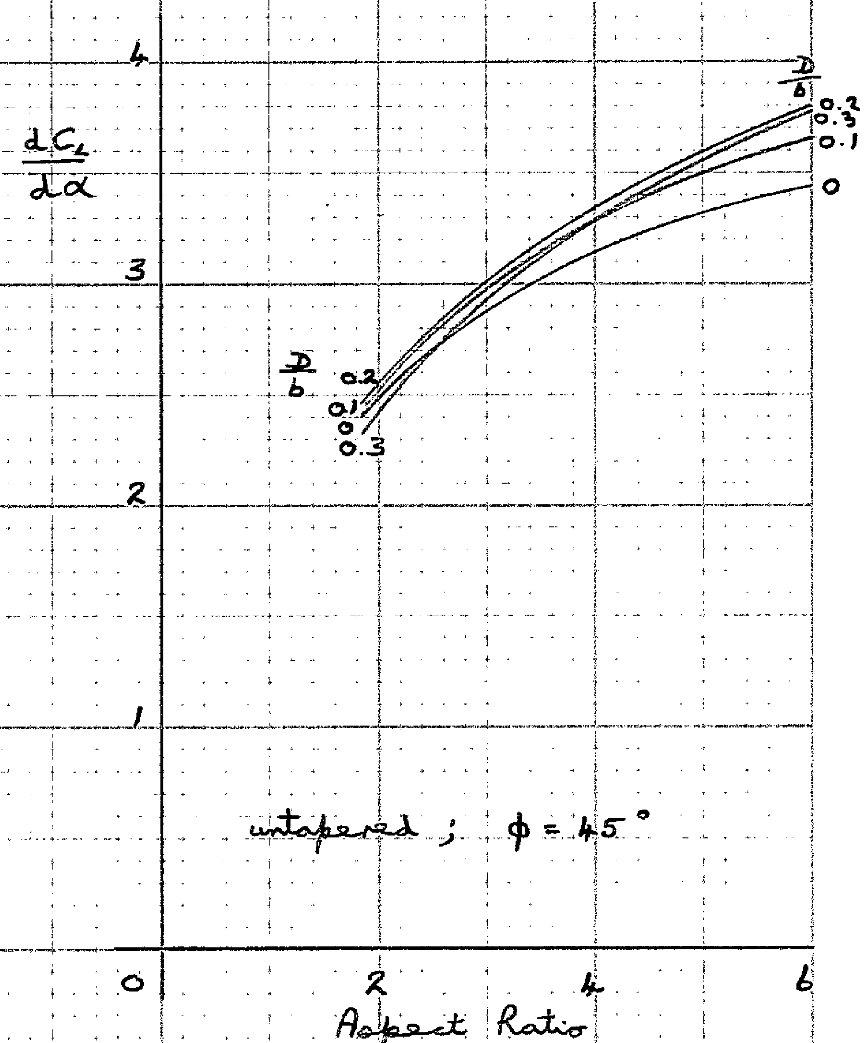

$\frac{dC_L}{d\alpha}$
4
3
2
1
0
2
4
6
Aspect Ratio
$\frac{D}{b}$
0.2
0.3
0.1
0
untapered; $\phi = 45°$

Fig. 12

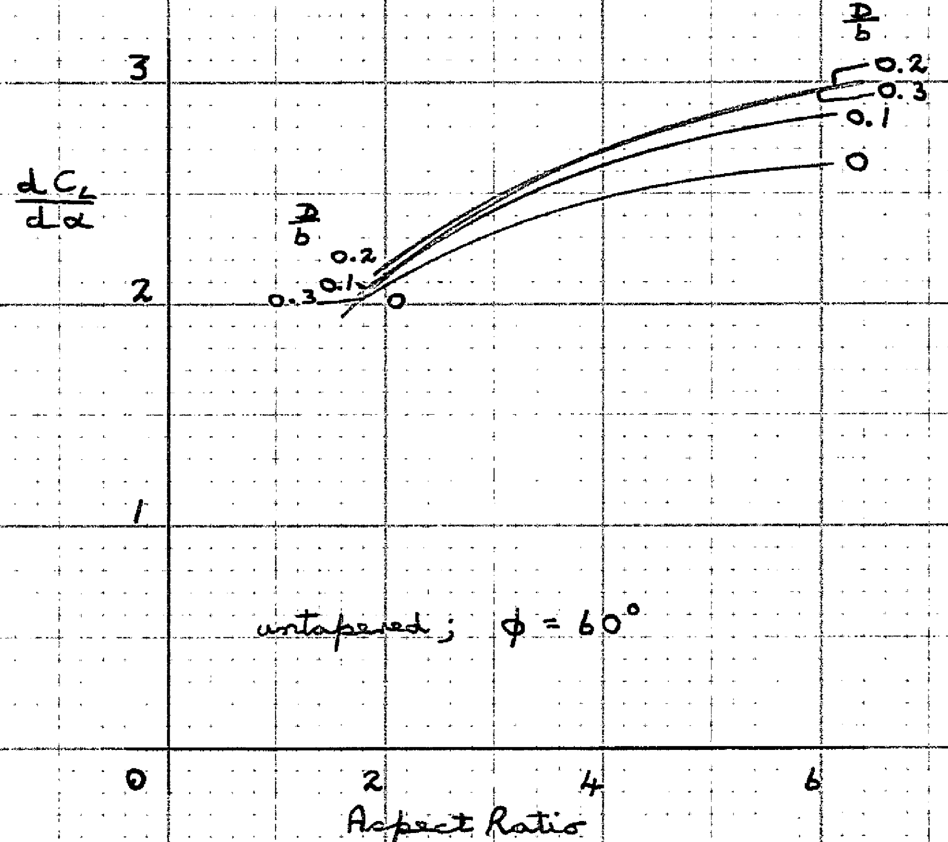

$\frac{dC_L}{d\alpha}$
3
2
1
0
$\frac{D}{b}$
0.2
0.3
0.1
0
$\frac{D}{b}$
0.2
0.1
0.3
0
untapered; $\phi = 60°$
2
4
6
Aspect Ratio

Fig. 13

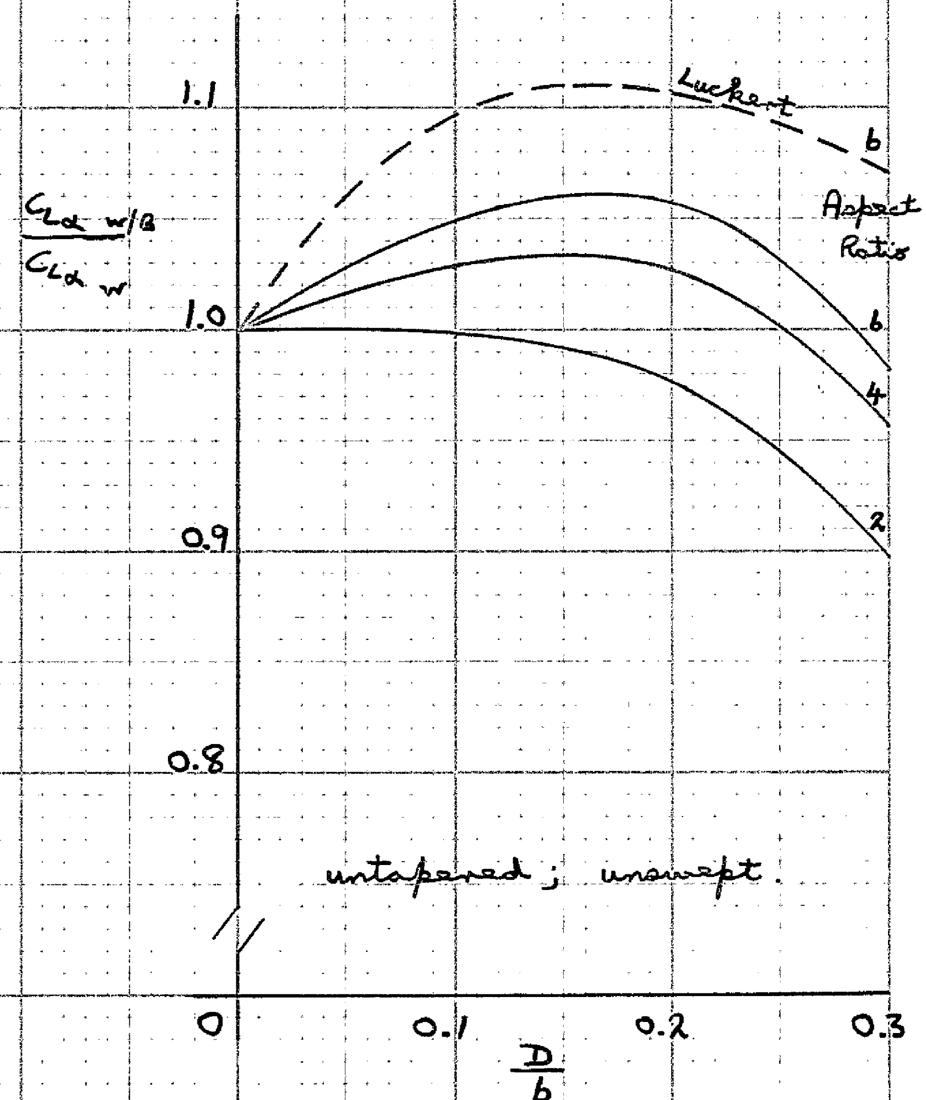

$\frac{C_{L\alpha\ w/B}}{C_{L\alpha\ w}}$
1.1
1.0
0.9
0.8
0
Luckert
6
Aspect Ratio
6
4
2
untapered; unswept.
0.1
0.2
0.3
$\frac{D}{b}$

Fig. 14

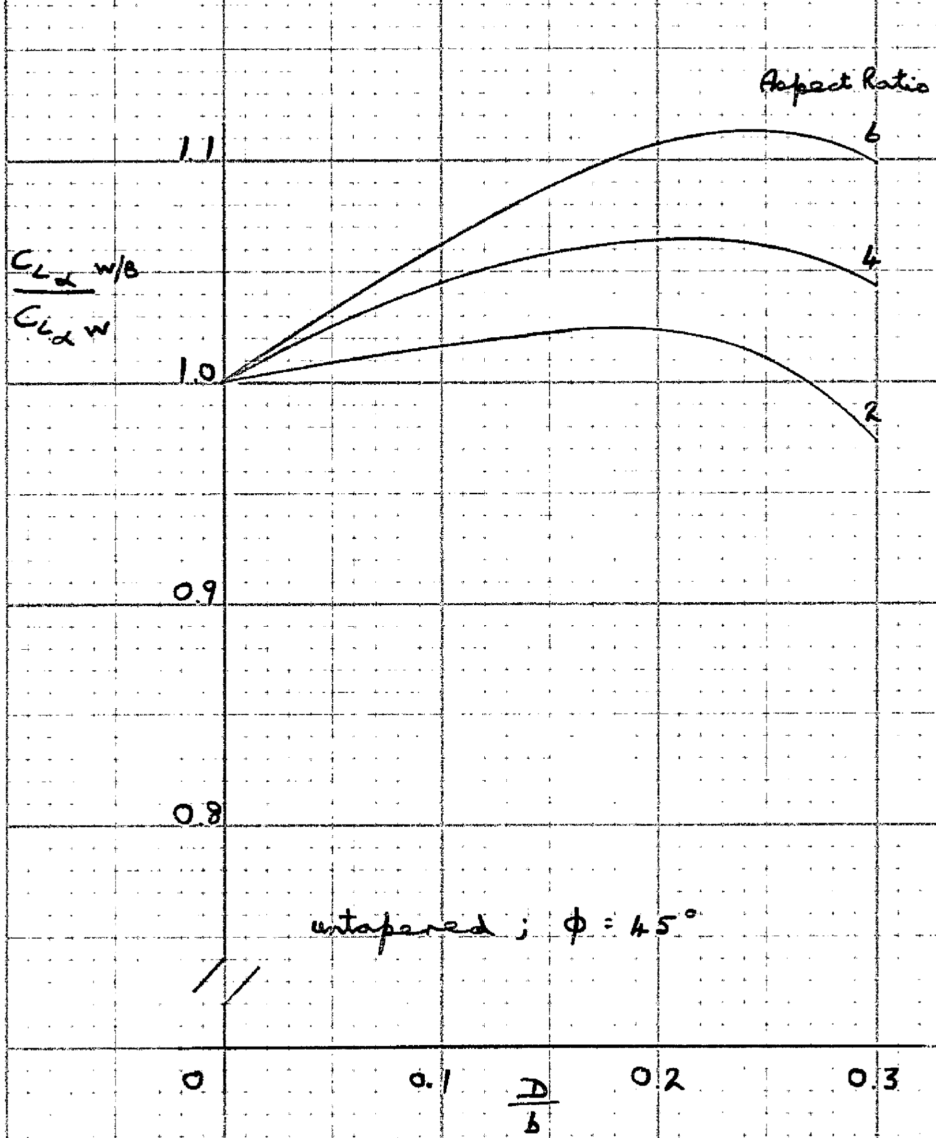

Aspect Ratio
6
4
2
1.1
1.0
0.9
0.8
$\frac{C_{L_\alpha}\ w/B}{C_{L_\alpha}\ w}$
untapered ; $\phi = 45°$
0
0.1
0.2
0.3
$\frac{D}{b}$

Fig. 15

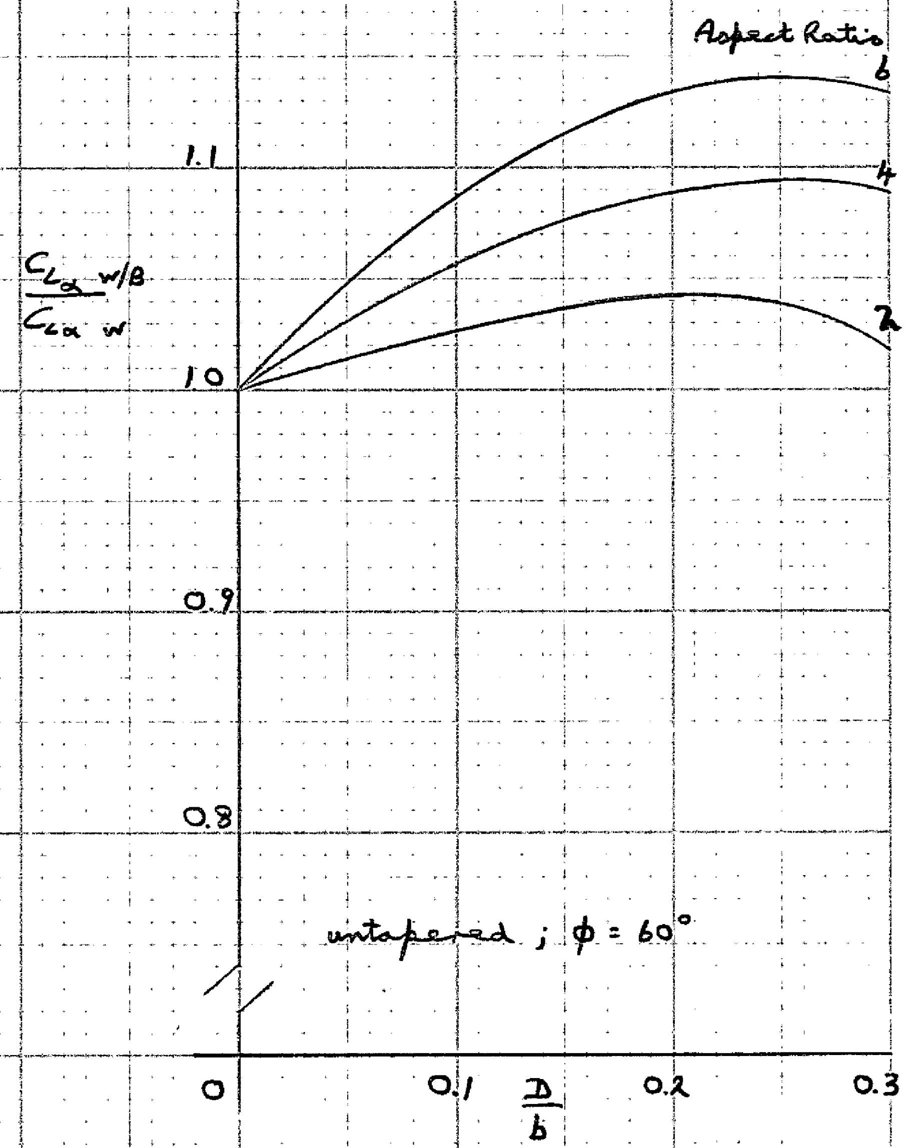

Aspect Ratio
6
4
2
1.1
1.0
0.9
0.8
$\frac{C_{L_\alpha}\ w/B}{C_{L_\alpha}\ w}$
untapered ; $\phi = 60°$
0
0.1
0.2
0.3
$\frac{D}{b}$

Fig. 16

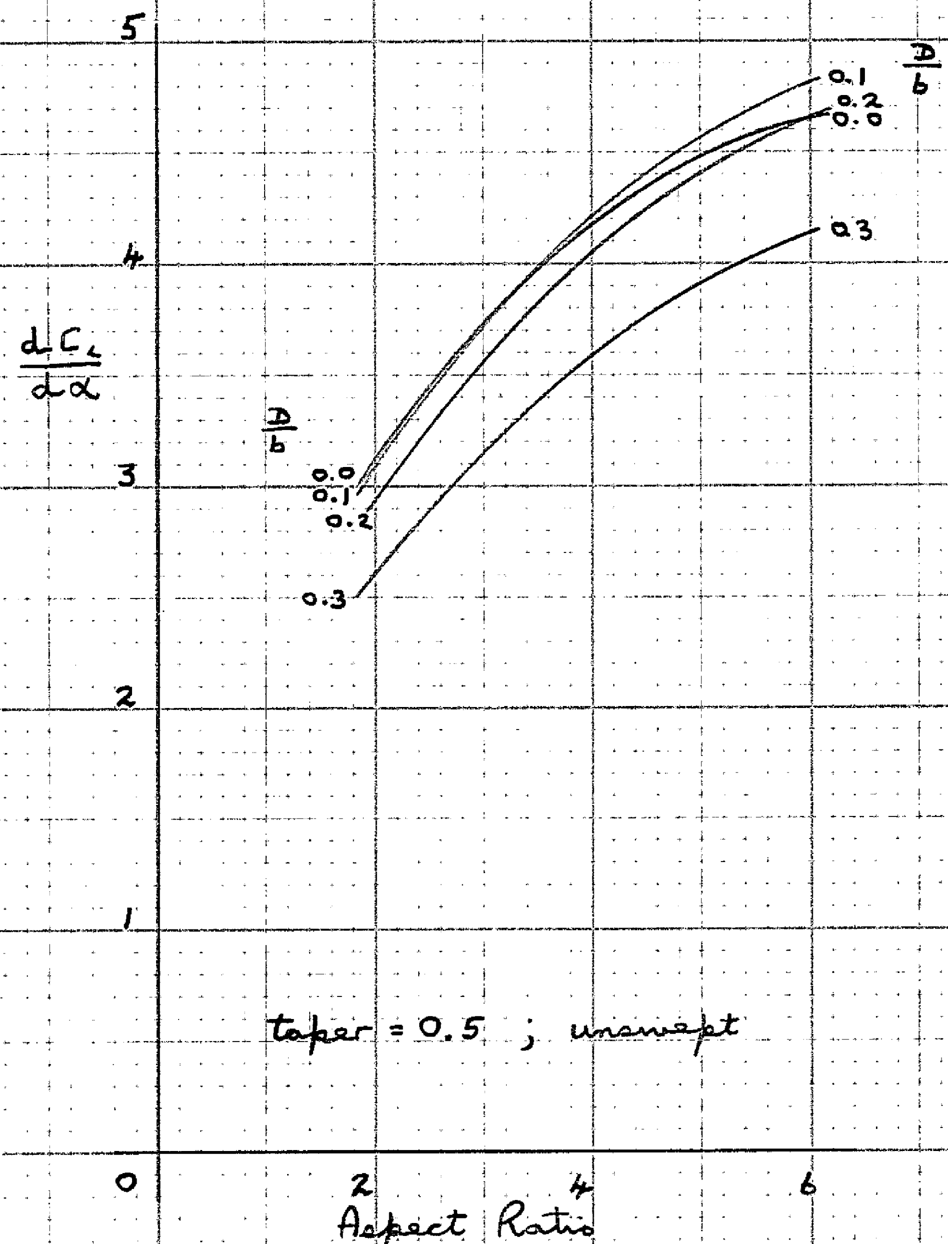

$\frac{dC_L}{d\alpha}$
5
4
3
2
1
0
$\frac{D}{b}$
0.0
0.1
0.2
0.3
0.1
0.2
0.0
0.3
taper = 0.5 ; unswept
2
4
6
Aspect Ratio

Fig. 17

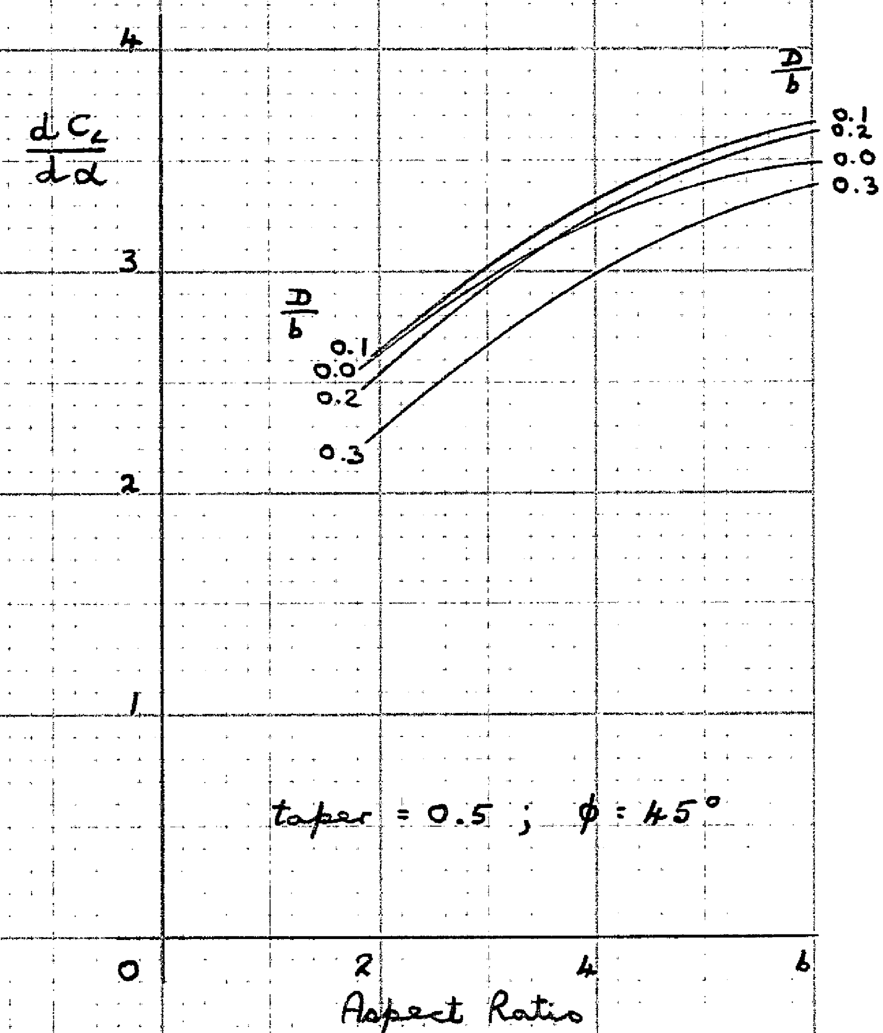

$\frac{dC_L}{d\alpha}$
4
3
2
1
0
$\frac{D}{b}$
0.1
0.0
0.2
0.3
0.1
0.2
0.0
0.3
taper = 0.5 ; ϕ : 45°
2
4
6
Aspect Ratio

Fig. 18

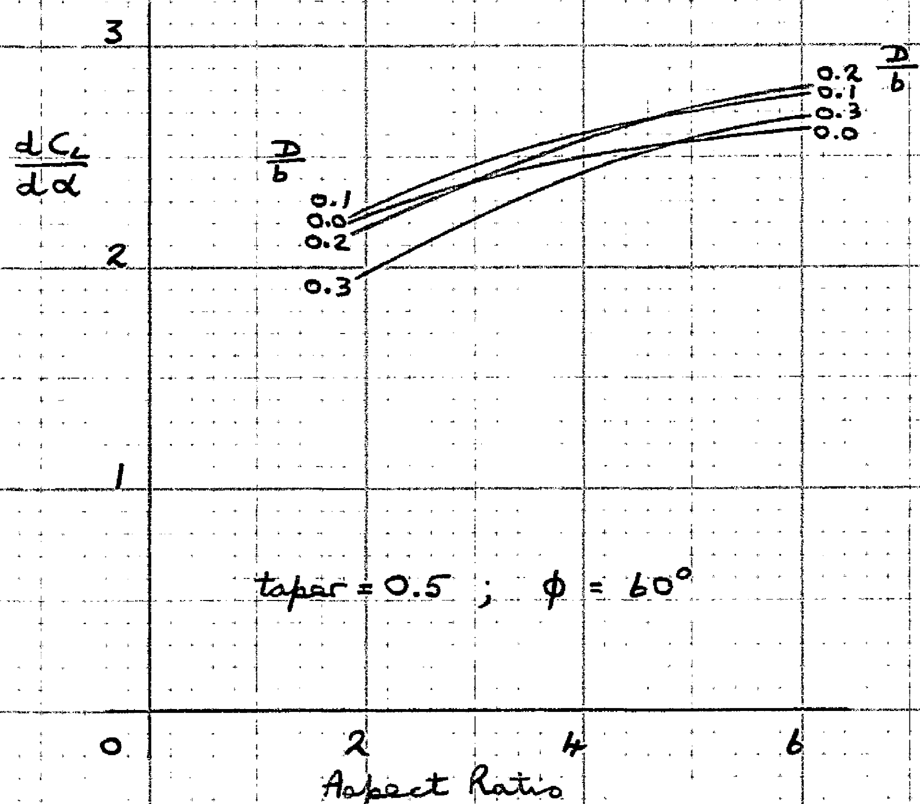

3
2
1
0
$\frac{dC_L}{d\alpha}$
$\frac{D}{b}$
0.1
0.0
0.2
0.3
0.2
0.1
0.3
0.0
2
4
6
Aspect Ratio
taper = 0.5 ; ϕ = 60°

Fig. 19

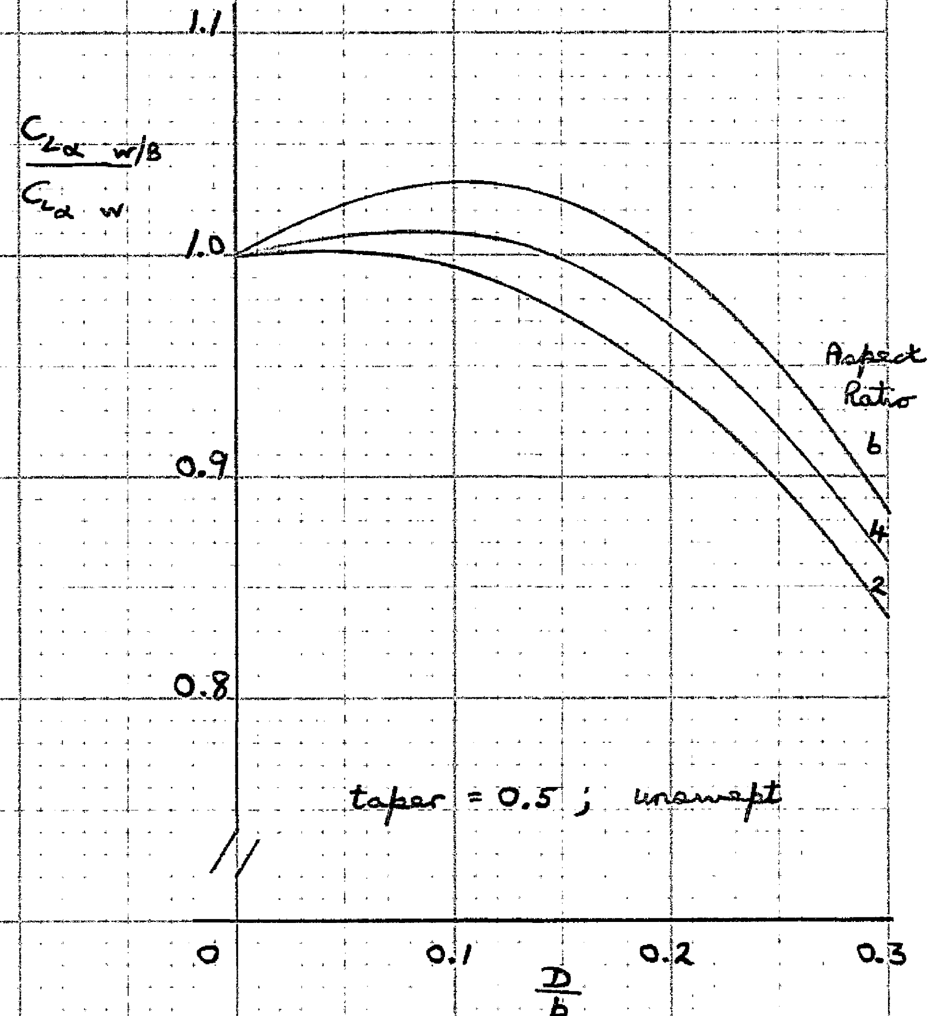

1.1
1.0
0.9
0.8
$\frac{C_{L\alpha\ w/B}}{C_{L\alpha\ w}}$
Aspect Ratio
6
4
2
0
0.1
0.2
0.3
$\frac{D}{b}$
taper = 0.5 ; unswept

Fig. 20

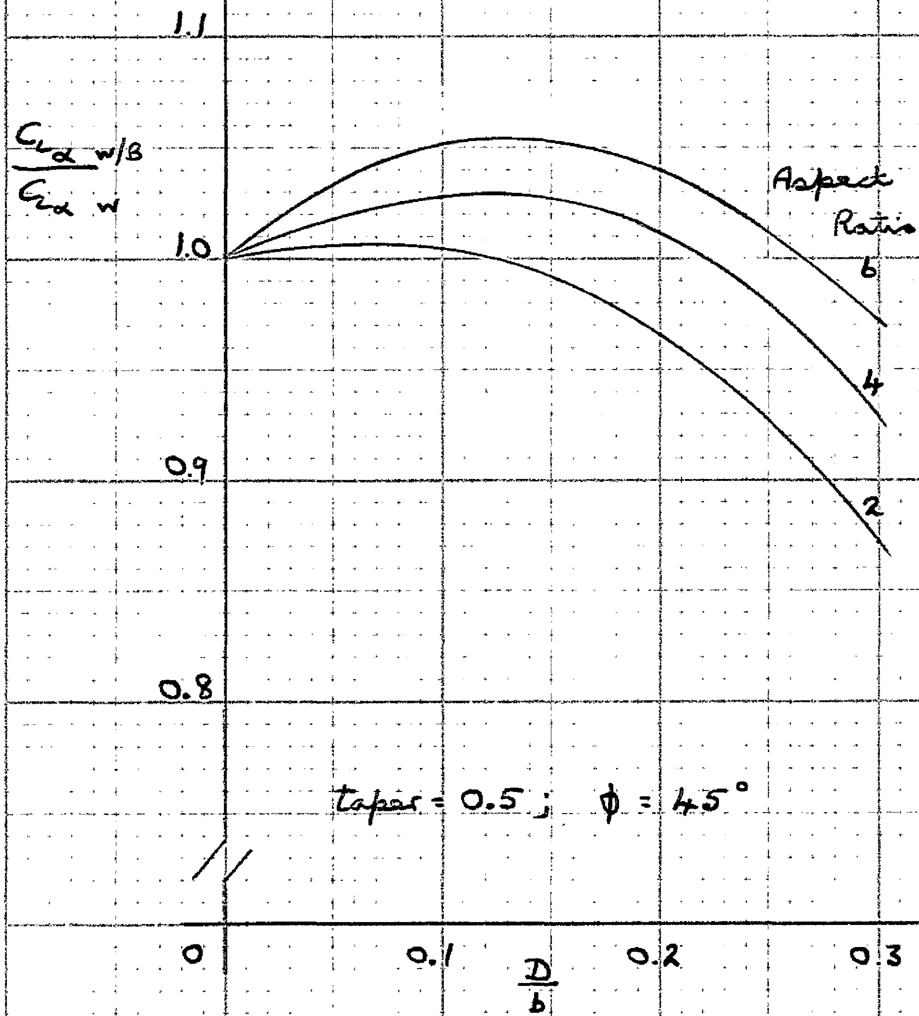

1.1
1.0
0.9
0.8
$\frac{C_{L\alpha}\ w/B}{C_{L\alpha}\ w}$
Aspect Ratio
6
4
2
tapar = 0.5 ; ϕ = 45°
0
0.1
0.2
0.3
$\frac{D}{b}$

Fig. 21

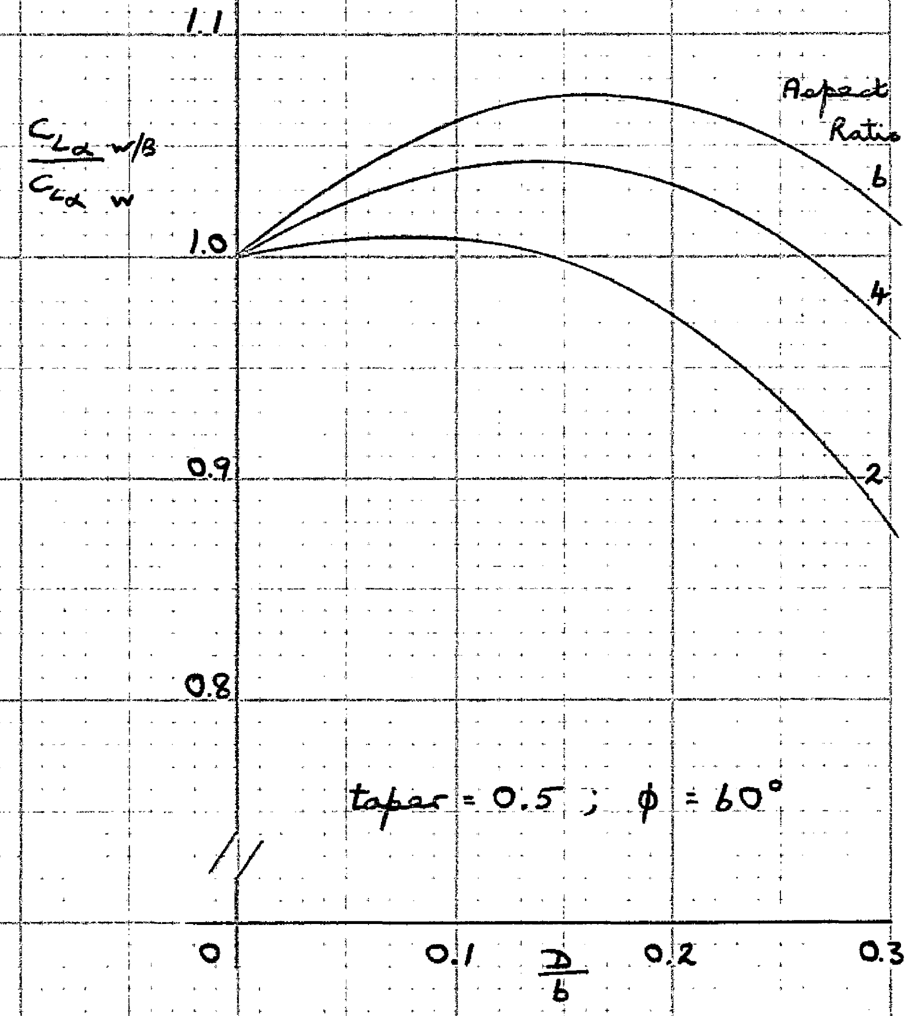

1.1
1.0
0.9
0.8
$\frac{C_{L\alpha}\ w/B}{C_{L\alpha}\ w}$
Aspect Ratio
6
4
2
tapar = 0.5 ; ϕ = 60°
0
0.1
0.2
0.3
$\frac{D}{b}$

Fig. 22

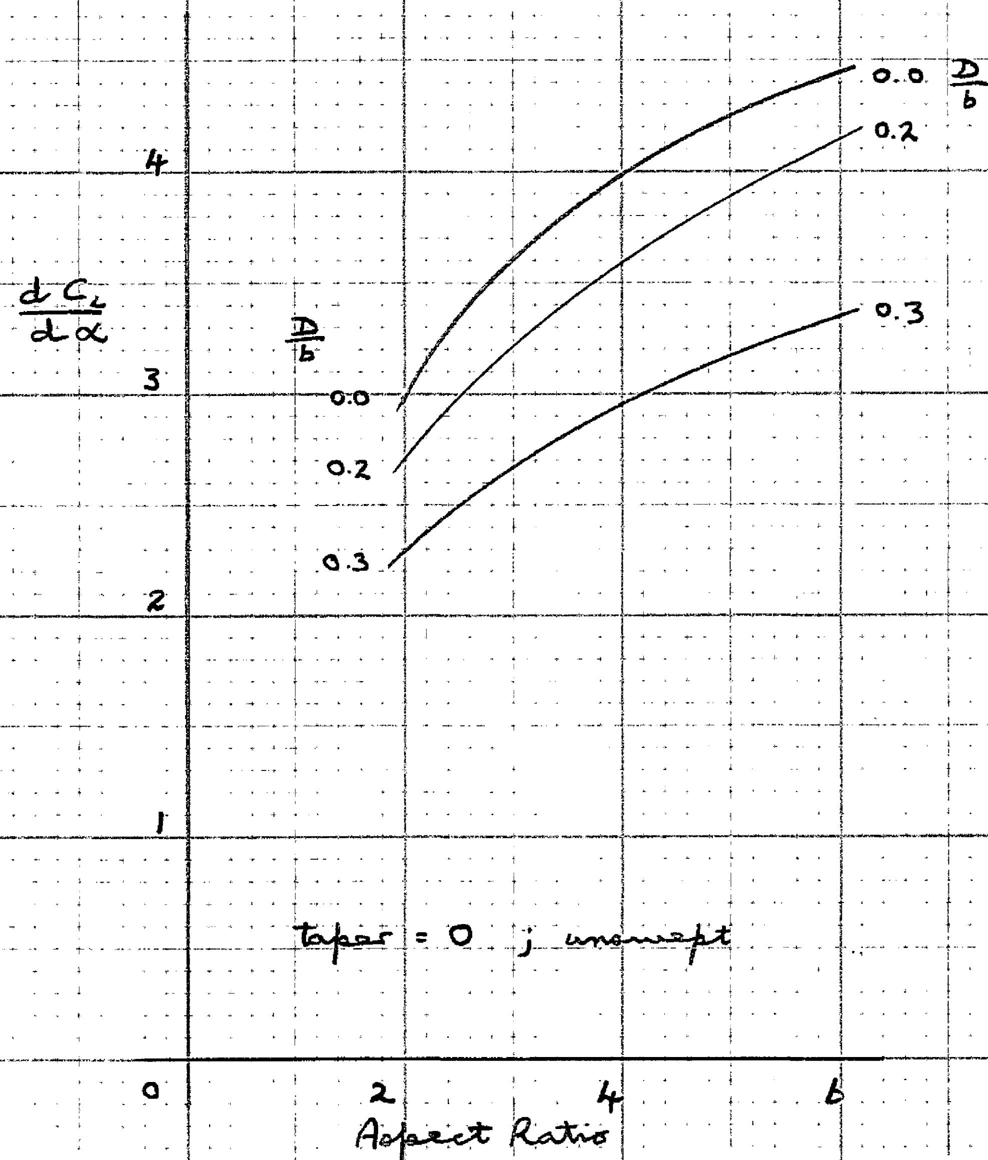

$\frac{dC_L}{d\alpha}$
4
3
2
1
0
2
4
6
Aspect Ratio
$\frac{D}{b}$
0.0
0.2
0.3
taper = 0 ; unswept

Fig. 23

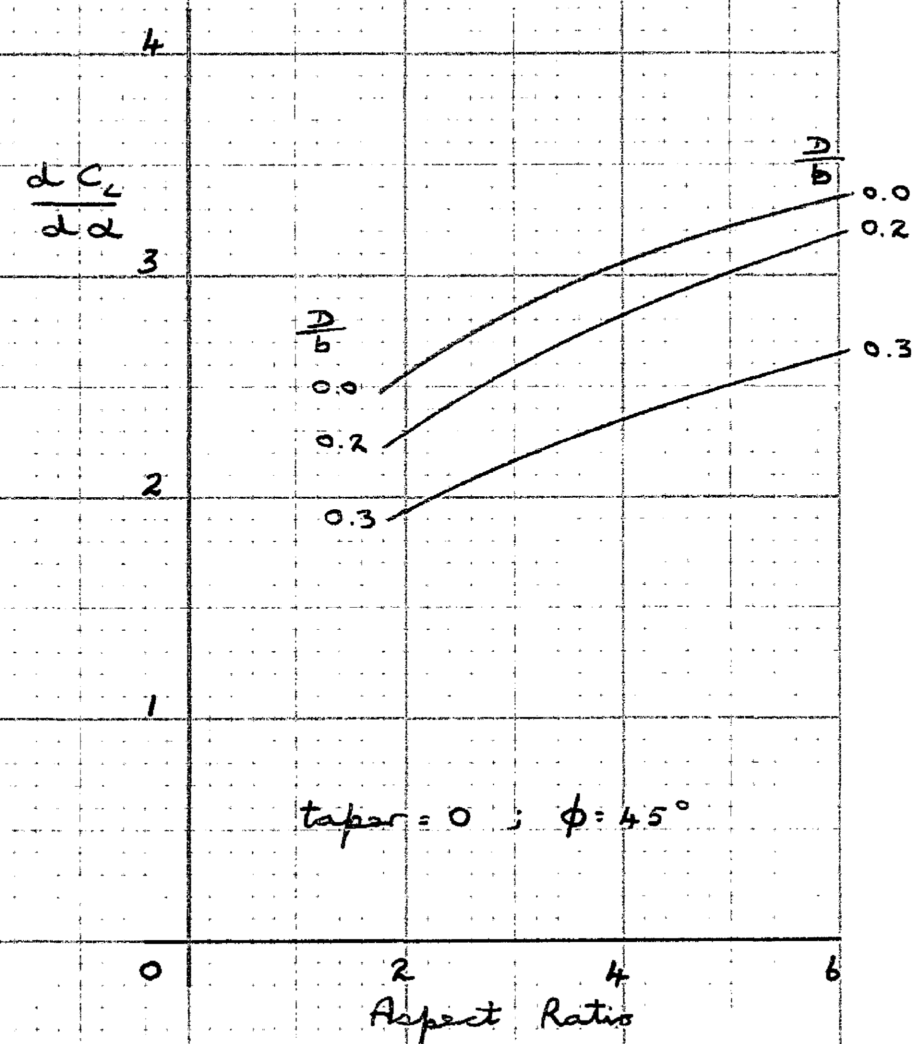

$\frac{dC_L}{d\alpha}$
4
3
2
1
0
2
4
6
Aspect Ratio
$\frac{D}{b}$
0.0
0.2
0.3
taper = 0 ; ϕ : 45°

Fig. 24

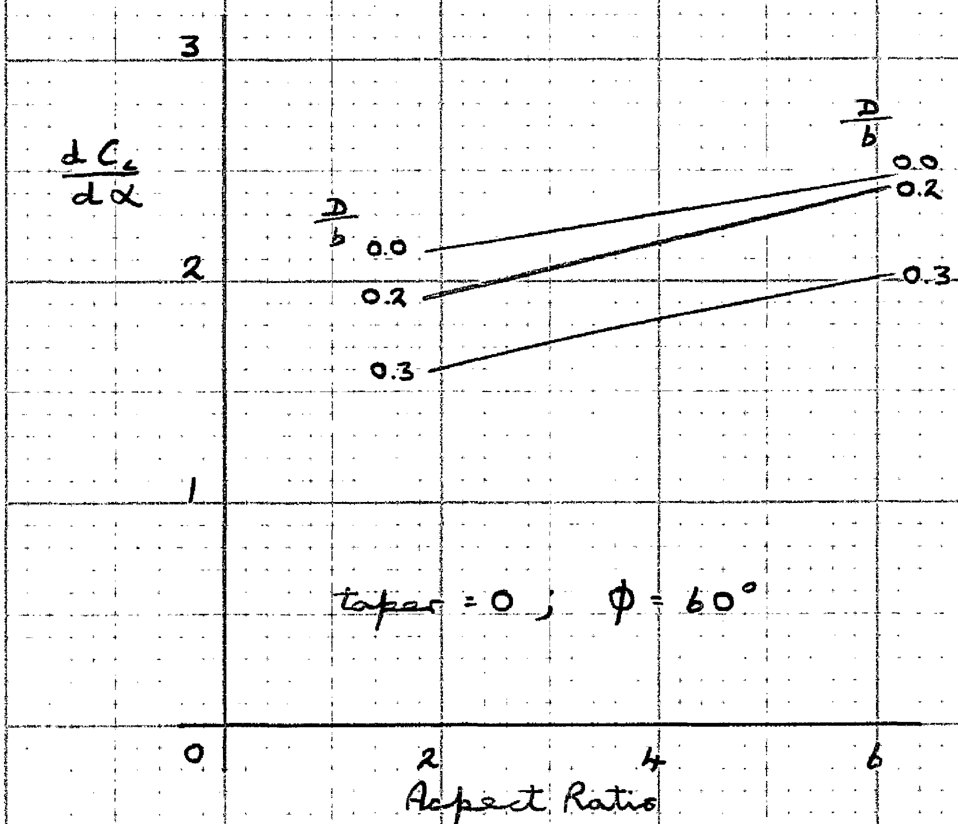

$\frac{dC_L}{d\alpha}$
3
2
1
0
$\frac{D}{b}$ 0.0
0.2
0.3
$\frac{D}{b}$
0.0
0.2
0.3
taper = 0 ; ϕ = 60°
2
4
6
Aspect Ratio

Fig. 25

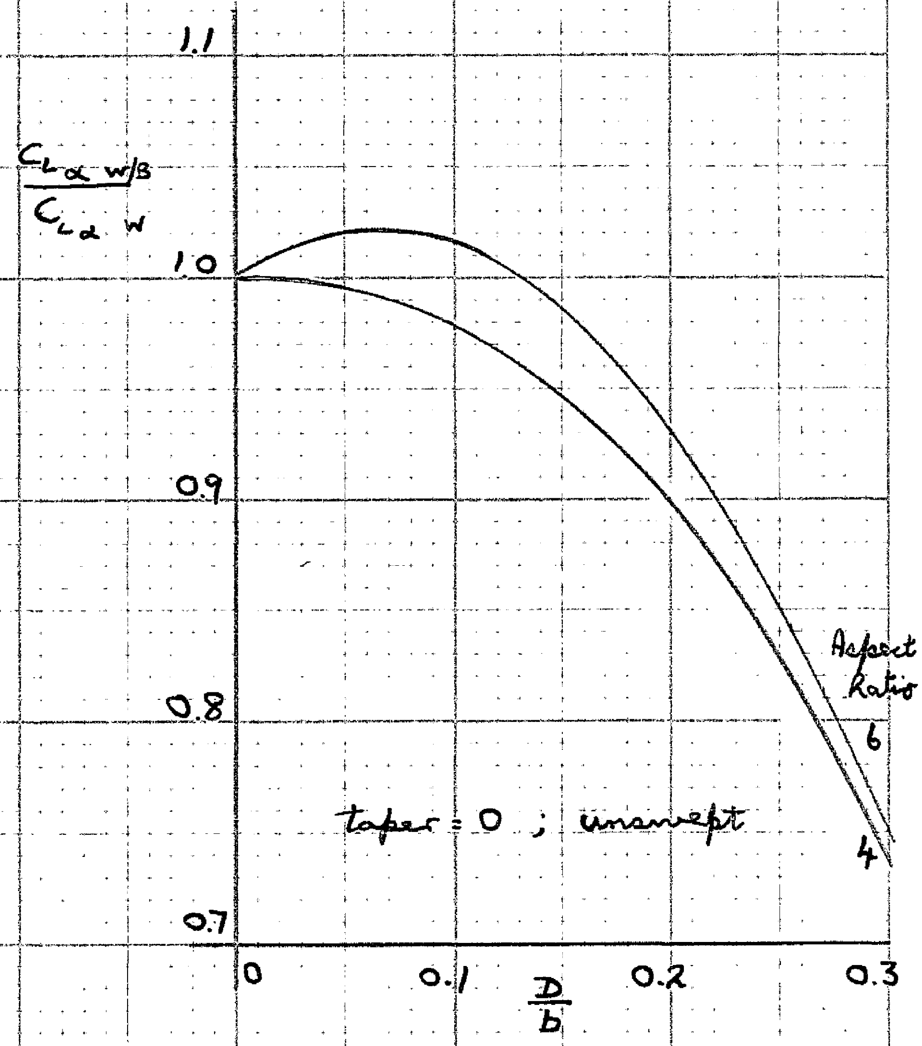

$\frac{C_{L\alpha\ W/B}}{C_{L\alpha\ W}}$
1.1
1.0
0.9
0.8
0.7
Aspect Ratio
6
4
taper = 0 ; unswept
0
0.1
0.2
0.3
$\frac{D}{b}$

Fig. 26

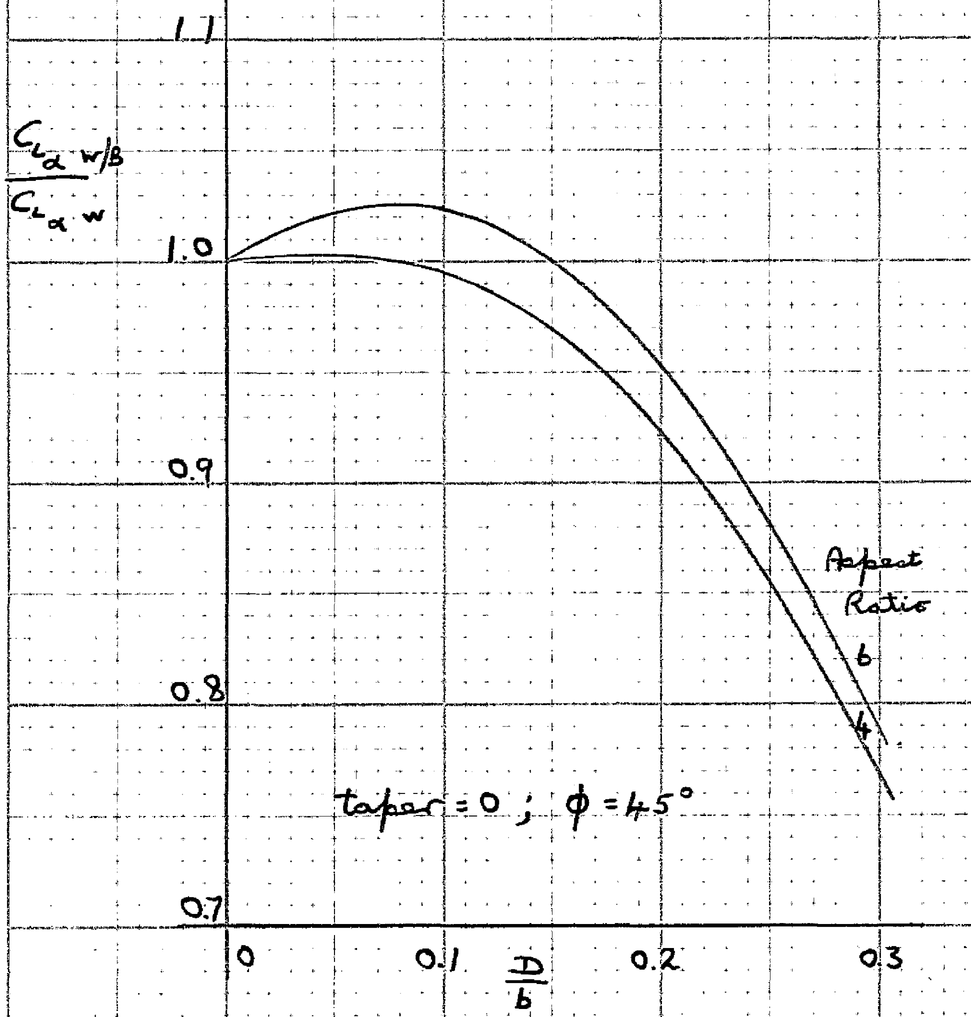

$\frac{C_{L_\alpha} w/B}{C_{L_\alpha} w}$
1.1
1.0
0.9
0.8
0.7
0
0.1
0.2
0.3
$\frac{D}{b}$
Aspect Ratio
6
4
taper = 0 ; ϕ = 45°

Fig. 27

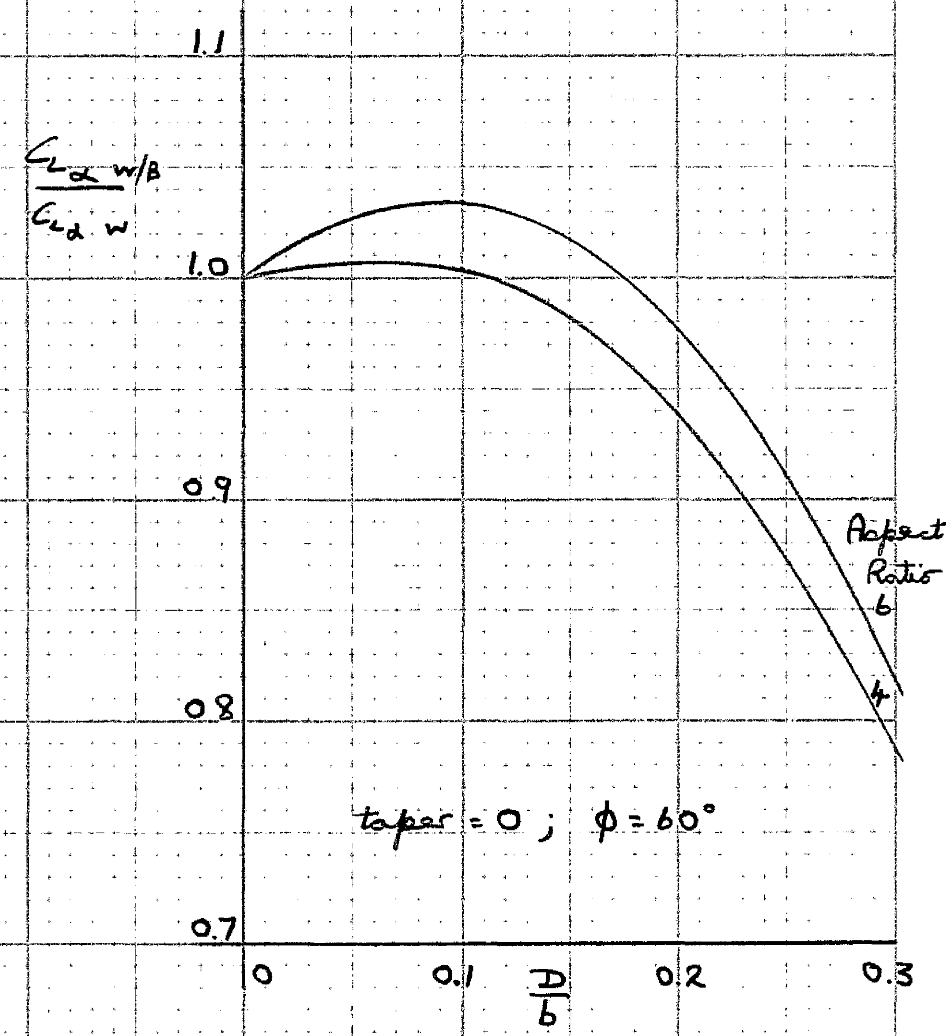

$\frac{C_{L_\alpha} w/B}{C_{L_\alpha} w}$
1.1
1.0
0.9
0.8
0.7
0
0.1
0.2
0.3
$\frac{D}{b}$
Aspect Ratio
6
4
taper = 0 ; ϕ = 60°

Fig. 28

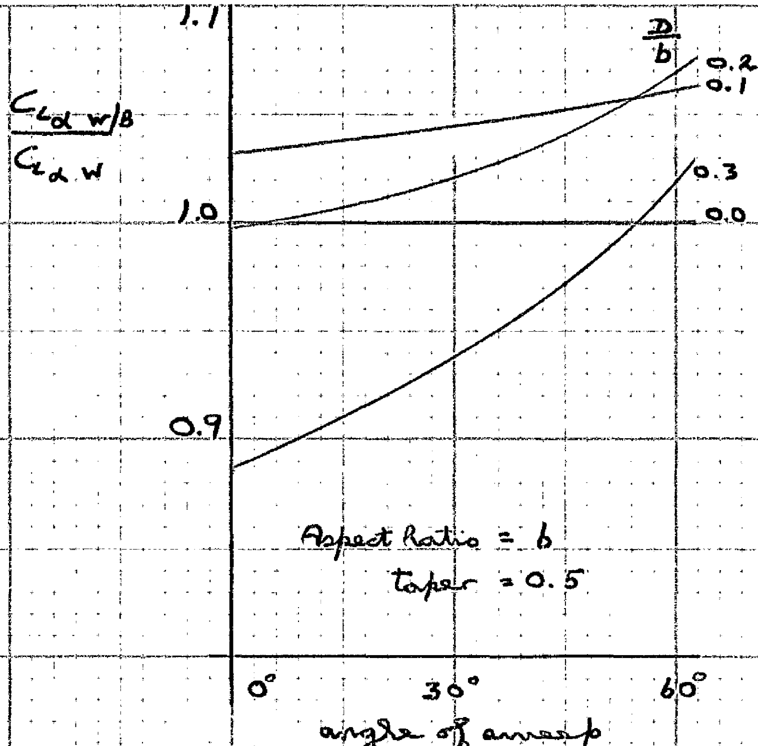

Fig. 29

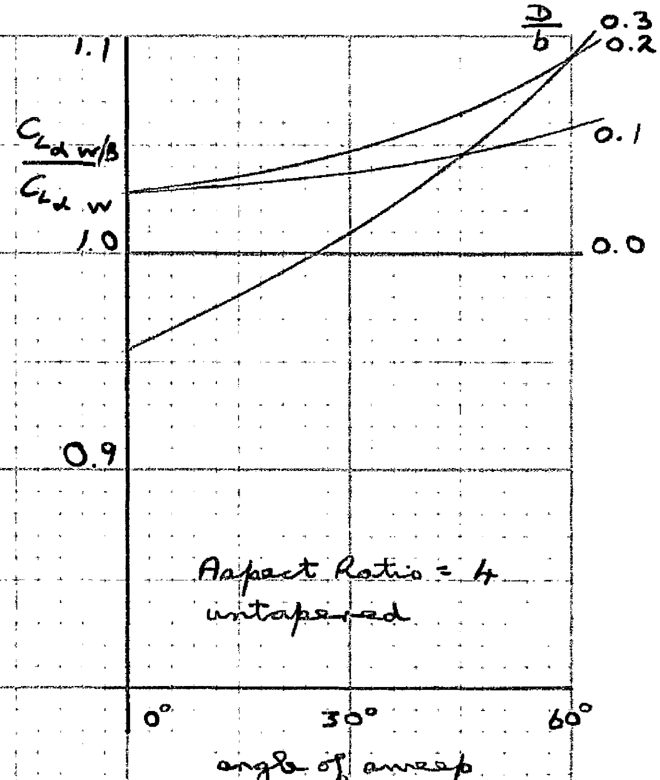

Fig. 30

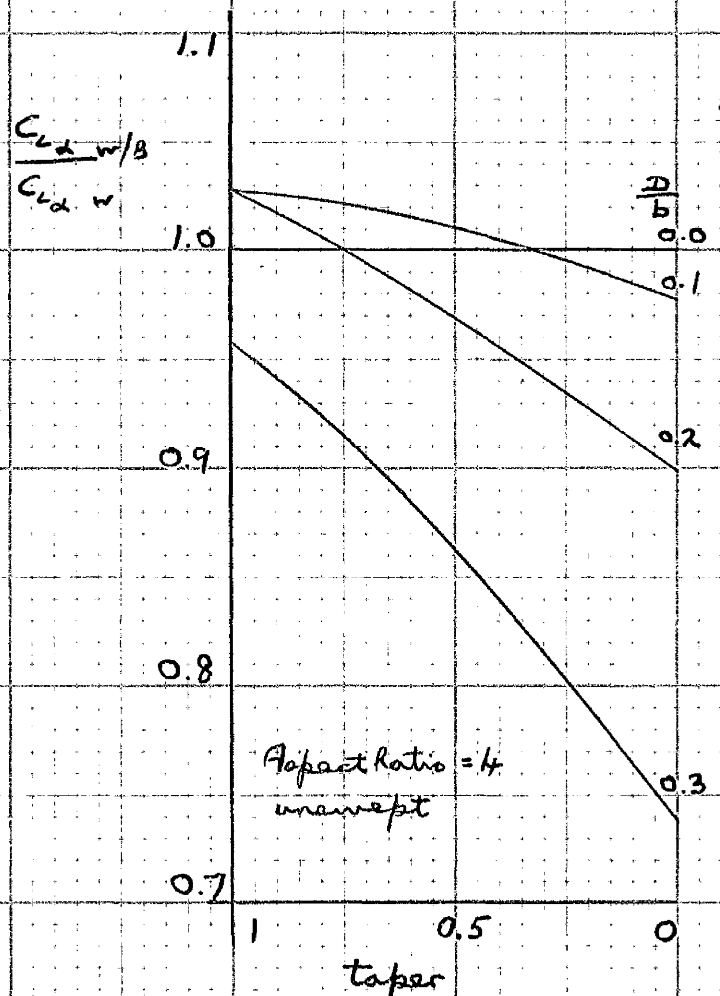

Fig. 31

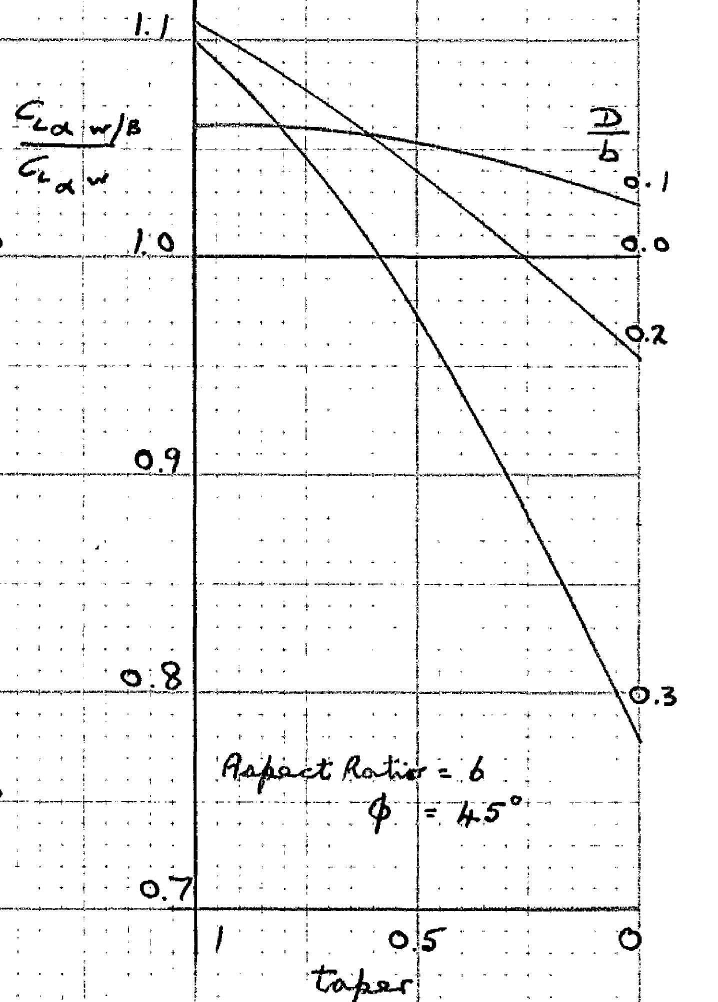

Fig. 32

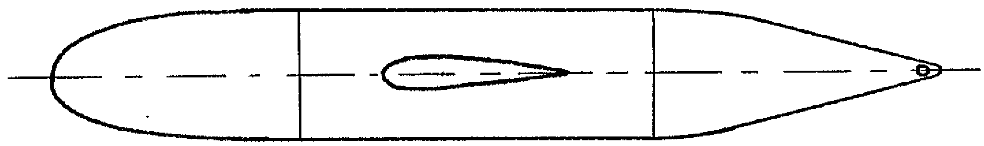

Fig. 33

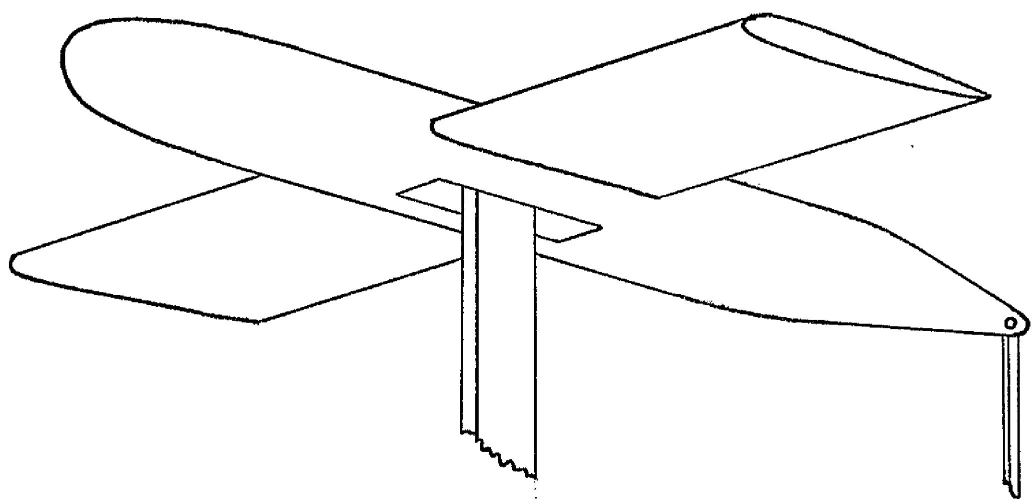

Fig. 34

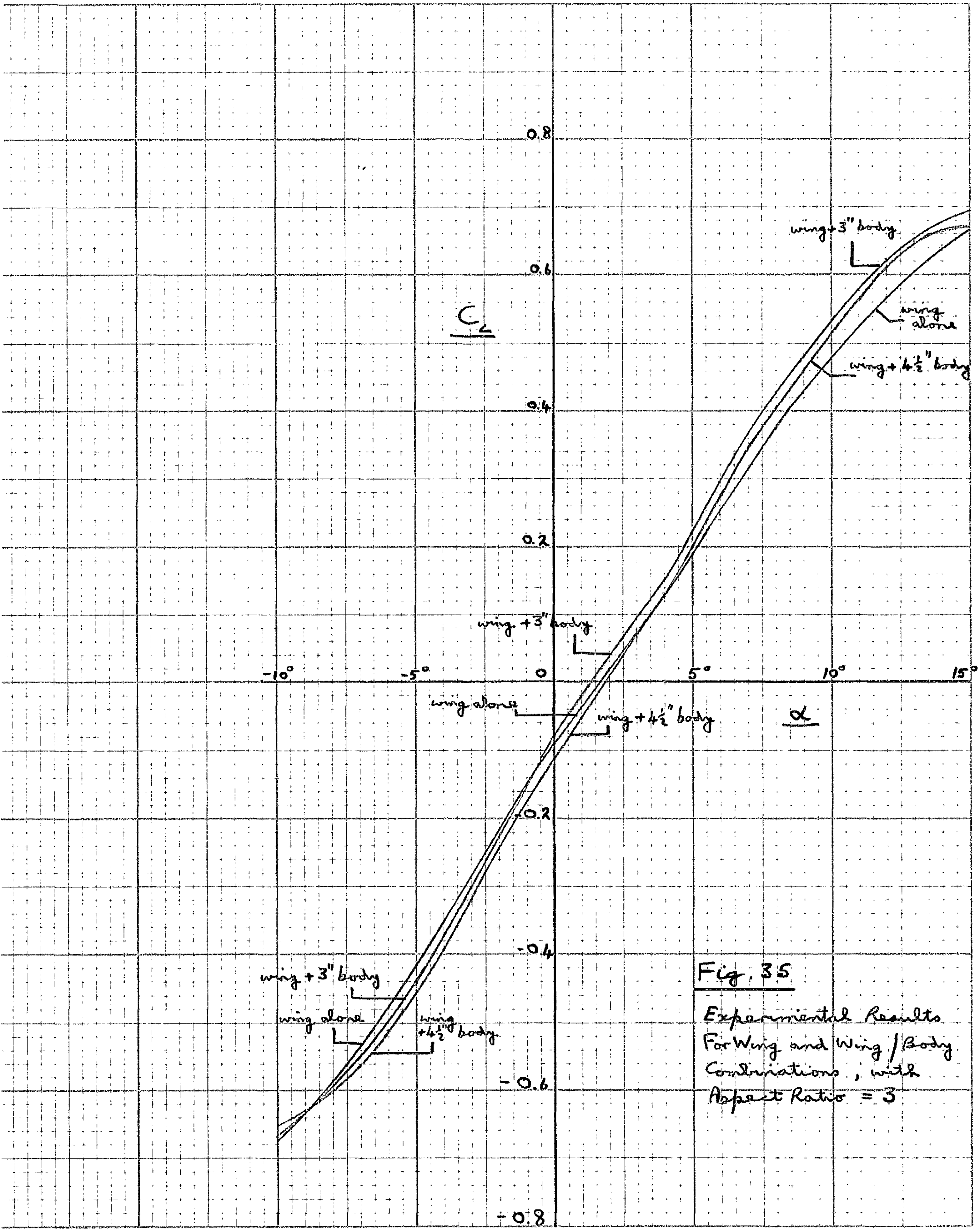

Fig. 35

Experimental Results For Wing and Wing / Body Combinations, with Aspect Ratio = 3

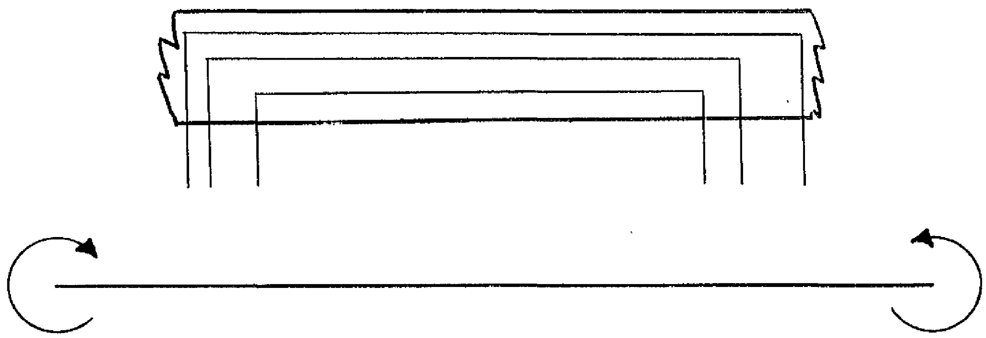

Fig. 36

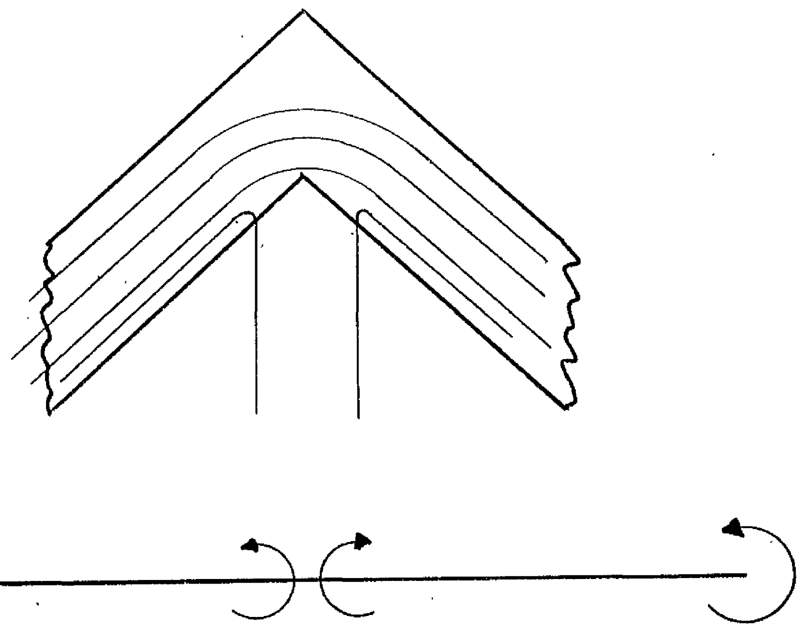

Fig. 37

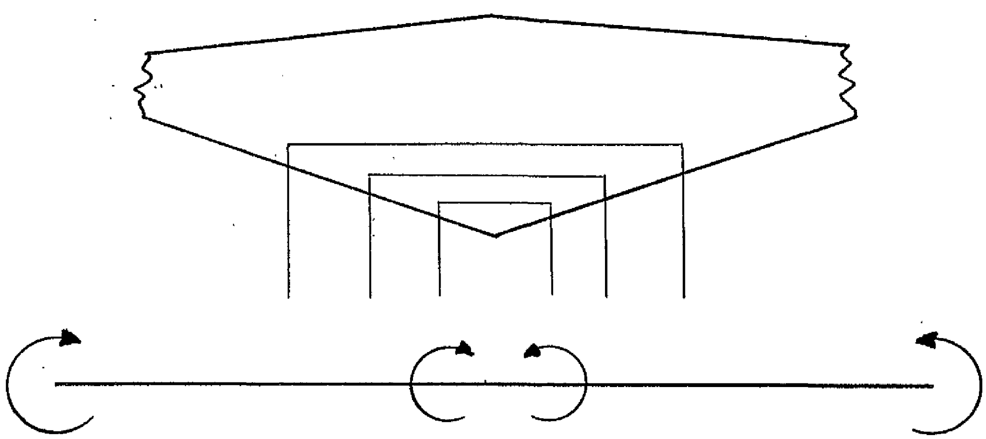

Fig. 38